

https://dspace.org/

# Powder metallurgy processing of high entropy alloys Bibliometric analysis and systematic review

**Olufemi Bamisaye; Michael Bodunrin; A.D Akinwekomi**

https://hdl.handle.net/10539/42023
WOS

Downloaded from a DSpace repository. https://dspace.org/

Review Article

Akeem Damilola Akinwekomi*, Olufemi Sylvester Bamisaye, and Michael Oluwatosin Bodunrin

# Powder metallurgy processing of high entropy alloys: Bibliometric analysis and systematic review

https://doi.org/10.1515/rams-2023-0188
received October 28, 2022; accepted February 12, 2024

**Abstract:** Research attention in powder metallurgy (PM) processing of high-entropy alloys (HEAs) is rising. Some reviews have been published but a detailed historical analysis to identify the thematic research areas and prospective future research areas is lacking. Therefore, this study presents a bibliometric literature analysis of PM-processed HEAs by mapping and clustering 700 articles published between 2007 and August 2022 in the Scopus database. The most prolific authors, their collaborators, institutions, and most preferred journals publishing PM-HEA works are identified and mapped. Publication trend shows that significant research attention in the PM processing of HEAs began to gain traction in 2016. The top three journals in this field are *Journal of Alloys and Compounds, Materials Science and Engineering A, and Intermetallics*. However, co-authorship network analysis does not reveal significant inter-institutional research collaboration indicating that strengthening this area could help to accelerate scientific discovery, enhance technology transfer, and commercialization of HEA products. Based on the co-occurrence frequencies of author keywords, popular research directions are identified, and a systematic review of emerging functional applications is undertaken. This work provides a comprehensive visual reference guide for researchers to deepen their knowledge of this field and delivers insight into prospective future research opportunities to stimulate further ground-breaking works.

**Keywords:** bibliometrics, high-entropy alloys, powder metallurgy, complex concentrated alloys, scientometrics

*** Corresponding author: Akeem Damilola Akinwekomi,** Department of Metallurgical and Materials Engineering, Federal University of Technology Akure, 340252, Akure, Nigeria,
e-mail: adakinwekomi@futa.edu.ng, akinwekomiad@gmail.com
**Olufemi Sylvester Bamisaye:** School of Chemical and Metallurgical Engineering, Faculty of Engineering and the Built Environment, University of the Witwatersrand, Johannesburg, South Africa; Mechanical Engineering Department, Faculty of Air Engineering, Air Force Institute of Technology, Kaduna, Nigeria
**Michael Oluwatosin Bodunrin:** School of Chemical and Metallurgical Engineering, Faculty of Engineering and the Built Environment, University of the Witwatersrand, Johannesburg, South Africa; DSI-NRF Centre of Excellence in Strong Materials, University of the Witwatersrand, Johannesburg, South Africa
ORCID: Akeem Damilola Akinwekomi 0000-0003-2943-3654

## 1 Introduction

Traditional alloys contain one main element with minor additions of other elements to impact different properties [1]. Hitherto, it is theorized that alloy systems with multi-principal elements will yield brittle intermetallic compounds with complex microstructures [1]. In 2004, two different research groups showed that new alloy systems with simple microstructures could be synthesized from multi-principal elements in equimolar or near-equimolar ratios [1–4]. These new alloy systems have come to be known as high entropy alloys (HEAs) [2] or multi-component alloys (MCA) [1,5] or compositionally complex alloys [6].

Various definitions exist for HEA/MCA. However, there are generally two acceptable ones based on composition and entropy. On the composition-based description, an HEA/MCA is defined as an alloy that contains five or more main elements whose composition vary between 5 and 35 atomic weight percent (at.%) [2,6,7]. The latter definition is derived from the configurational entropy ($S$), which describes an HEA/MCA as an alloy with five principal elements in equimolar concentration, such that its $S \geq 1.61R$ (where $R$ is the standard gas constant) [8].

The vast majority of existing HEA/MCA is processed *via* casting or generally from the liquid state *via* arc melting [1,2,9–11]. As the processing temperature can be greater than 3,000°C, for instance in arc melting, elements with low melting points (*e.g.*, Mg and Zn) may evaporate, thus making it difficult to precisely control the composition of the HEA/MCA [12]. Furthermore, coarsening, and elemental segregation may also occur. For instance, Cu is known to

Open Access. © 2024 the author(s), published by De Gruyter. This work is licensed under the Creative Commons Attribution 4.0 International License.

segregate from other elements due to its positive mixing enthalpy with many elements [13]. In addition, this route may not be compatible with the existing industrial processes due to the high cost of equipment, and limitation in product shape and size [14].

Compared with the liquid state process, solid state processing *via* powder metallurgy (PM) can overcome some of these challenges. PM-based processing has the capability of producing non-equilibrium phases, more homogenous grain structure [15–23]. It also offers enhanced stability of solid solution phases due to increased configurational entropy even in immiscible systems [16]. Besides, PM can be used to process elements with different melting points, and thus evaporation of low melting point elements is avoided [24,25]. In addition, the PM *via* mechanical alloying approach is quite suitable for synthesizing nanocrystalline alloys, which is otherwise extremely difficult using the common melt/casting technique [26].

Solid state processing techniques include mechanical alloying/high-energy ball milling of elemental or pre-alloyed powders [4,26–30], and recent techniques like additive manufacturing [31–34]. After the powder processing stage, the alloy so-obtained is densified through various consolidation processes including spark plasma sintering (SPS) [25,26,29,35], microwave sintering [4,29,36], and vacuum hot pressing [24,37].

Despite that PM-based processing of HEA/MCA is relatively new, the number of published articles is increasing at a rapid rate. It is, therefore, important to synthesize the accumulating knowledge in this field and keep abreast of new information. Consequently, a few review studies [16,38] have been published to summarize some key findings on the PM processing of HEA/MCA. While Torralba and co-workers [38] have reviewed the broad area of PM processing of HEA/MCA, Vaidya *et al.* [16] chose to examine the aspect of mechanical alloying, one of the main routes in PM processing. A relatively recent work examines additive manufacturing of PM [39]. However, there is a dearth of data-driven bibliometric works dedicated to assessing, investigating, and visualizing the PM-HEA/MCA literature from a global perspective. Additionally, new findings not covered in the earlier review works, especially on functional applications and deformation mechanisms, are investigated in this present study.

Bibliometric review, also known as science mapping or scientometrics, is premised on text/data mining techniques to analyze and visualize different types of bibliometric networks based on the outputs of the academic literature in a particular scientific field [40]. The analysis is done through the application of mathematics and statistical methods, as originally defined by Pritchard [41]. The dynamics of the development of science and technology is premised on citation, which establishes the linkages between researchers, their ideas, publication outlets, as well as institutions [42]. This idea was pioneered by Eugene Garfield, who proposed the idea of Science Citation Index [43,44]. Ever since, bibliometrics has been deployed for the evaluation of research performance and distribution of research funding at different levels, from individuals/groups to universities/institutions [45]. For a good perspective on the history of bibliometrics/scientometrics, the reader is referred to these works [42,44]. One of the advantages of a bibliometric review is that it may overcome the subjectivity associated with the findings of narrative and systematic reviews [46] or peer reviews [45]. Furthermore, bibliometric mapping helps to understand the historical and evolutionary changes in a research field [47], assists experts in enriching their knowledge of a certain field [48], and creates a comprehensive visual reference platform for future researchers. Some of the research fields that have benefitted from bibliometric reviews include computational intelligence [49], medicine [50], library and information science [47], microbial fuel cell [51], and conversion technologies for carbon dioxide [52]. However, no such review has been undertaken on PM-based HEA/MCA materials. It is important to conduct a detailed historical analysis of the development in the field of PM-based HEA/MCA and identify current research themes and areas needing further research activities.

Therefore, this present work serves to fill this gap by employing text-mining methodology and bibliometric visualization techniques to analyze the literature on PM processing of HEA/MCA from 2007 to August 2022 using the VOSviewer software [53]. The main objectives of this study are to: (i) analyze the trend of scientific publications in the PM-processing of HEA, (ii) identify scientific collaboration networks of researchers, institutions, and countries, (iii) create a mapping of co-occurrence networks of keywords to evaluate different research themes and directions, and (iv) evaluate high impact publication outlets with a view to reviewing some emerging functional application fields. Further, this will help to identify prospective research directions and development to stimulate further studies in this field. Additionally, this work will serve as a template for analyzing the application of bibliometrics to a niche in the HEA field. This work is structured as follows: Section 2 discusses the methodology of article retrieval and bibliometric analyses, while the results of the bibliometric analysis of the literature on PM-HEAs are presented in Section 3. A brief review of some deformation studies and selected emerging functional applications of PM-processed HEAs are contained in Section 4. Sections 5 and 6 contain suggested future works and conclusions, respectively. This study will be of immense benefit to researchers by providing a comprehensive visual

reference guide to comprehend the extent of work on-going in the field, enhance research collaboration, and identify prospective future research directions.

## 2 Methods

Bibliometric analysis utilizes outputs of the academic literature in a particular scientific field study to create networks of citations relationship between authors, journals, countries, co-authorship analysis of authors, or co-occurrence of keywords [40].

### 2.1 Data mining strategy

The schematic flow chart in Figure 1 shows the steps undertaken to complete the bibliometric analysis and systematic review in this work. All the articles published between 2007 and August 2022 were searched and retrieved from the Scopus database. Although Web of Science offers similar coverage, Scopus offers a wider and more extensive coverage of the abstracts and citations of the peer-reviewed literature [51]. Some keywords related to PM and HEA/MCA were utilized in searching the title, abstract, and keyword fields in Scopus. The query string utilized was (TITLE-ABS-KEY ("high entropy alloy*" OR "multicomponent alloy*" OR "multiprincipal element alloy*" OR "composit* complex alloy*") AND TITLE-ABS-KEY ("powder metallurgy" OR "powder technology" OR "hot press*" OR "hot isostatic press*" OR "HIP" OR "hot consolidat*" OR "sinter*" OR "spark plasma sinter*" OR "SPS" OR "ball mill*" OR "mechanical mill*" OR "mechanical alloy*" OR "mechanical activation" OR "solid state processing" OR "powder metallurg*" OR "PM" OR "powder process*") AND NOT TITLE-ABS-KEY ("binary" OR "glass" OR "glass form*" OR "glass-form*" OR "steel" OR "equilibrated" OR "binary alloy" OR "ternary" OR "equivalent" OR "super alloy*: OR "superalloy" OR "Inconel") AND NOT SRCTITLE ("glass*" OR "glass-form*" OR "glass form*") AND LANGUAGE (English)) AND PUBYEAR > 2003 AND (LIMIT-TO (SRCTYPE , "j")) AND (LIMIT-TO (DOCTYPE, "ar")) AND (LIMIT-TO (LANGUAGE, "English")). With this query string, 700 articles were extracted from the database. The metadata of the selected literature were extracted from the database on 22nd August 2022.

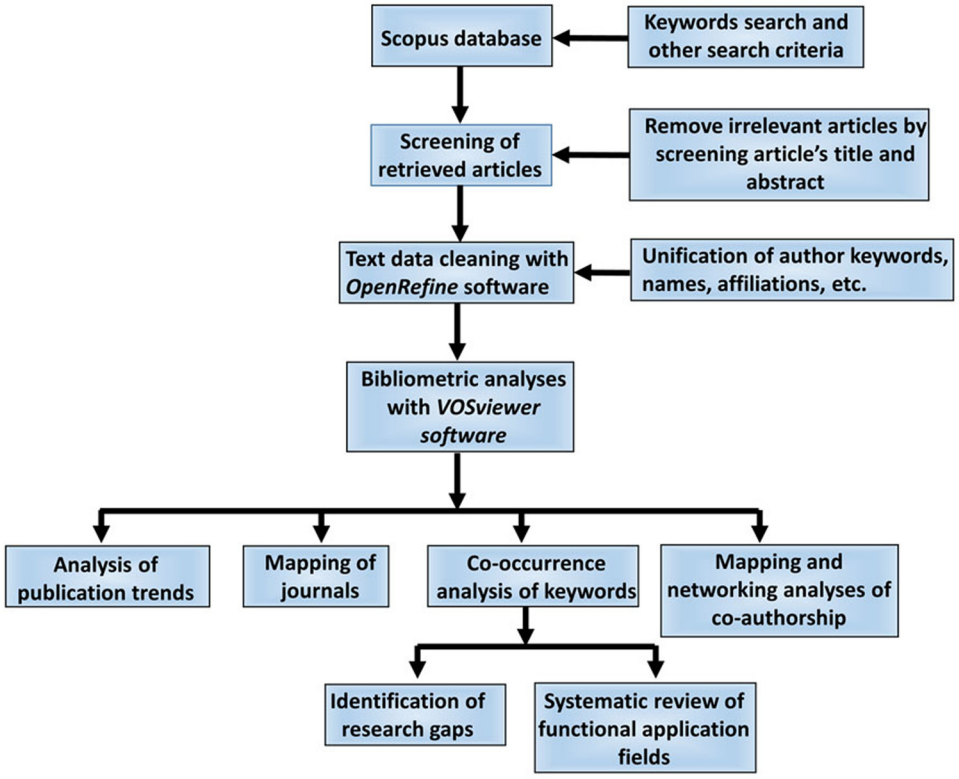


**Figure 1:** Schematic flow chart for bibliometric analysis.

## 2.2 Text cleaning/data reconciliation

The title abstract, and keywords of the retrieved 700 articles were screened to detect and eliminate unrelated ones. No irrelevant article was found, so all the700 articles were subjected to further text cleaning and bibliometric analyses. In the text cleaning step, various forms of author keywords were unified. For instance, keywords like "high-entropy," "HEA," "high entropy," and "high entropy alloy" were combined and treated as *high entropy alloys*. Likewise, "powder metallurgy," "powder processing," and "powder technology" were combined as *powder metallurgy*. Furthermore, author keywords such as ("SPS," "spark plasma sintering); ("oxidation," "oxidation kinetics," "oxidation resistance"); and ("wear," "wear behaviour," "wear resistance," "wear mechanisms") were grouped as *spark plasma sintering, oxidation behavior,* and *wear,* respectively. Text cleaning was accomplished with a freely available software, OpenRefine, v. 3.4.1 [54].

## 2.3 Bibliometric analyses

After cleaning the data of the articles, they were analyzed to investigate the trend of publication growth over the years. Further, bibliometric analyses comprising network maps of co-occurrence of article keywords (*i.e.*, author keywords), co-citation between articles, co-citation between scientific journals, and co-authorship between countries were undertaken. These were deployed to identify the main research interest and direction, citation pattern, influential outlets for scientific works, and scientific collaboration between institutions and countries. For these analyses, a free, open-source science mapping software VOSviewer 1.6.17 was utilized [53]. VOSviewer is a distance-based map wherein the relationship between items is reflected by the length of the distance between them. Invariably, a shorter distance between two items indicates a strong relationship between them. Thus, it is easier to identify clusters of related items [53]. Furthermore, each item of analysis (journal, author, country, *etc.*) is represented by a node (circle or rectangle). The larger it is, the more influential/important the item is. The importance of an item may be assessed based on for instance, the number of documents, citations, average citations, *etc*. Items with the same color belong to the same cluster and thus, indicates their co-citation of HEA/MCA research. Maps displayed based on density visualization, *e.g.*, for journals, indicate that they received a lot of citations or published more articles [53].

# 3 Results and discussion of bibliometric analysis of literature on PM processing of HEA/MCA

## 3.1 Trend of scientific publication on PM processing of HEA/MCA from 2004 to August 2022

Figure 2 shows the annual scientific outputs on PM-based processing of HEA/MCA. According to the Scopus database, one article is published per year from 2007 to 2011. However, in 2013, the number of research articles have increased significantly to 12. This increasing trend is equally observed in subsequent years until 2020 when the number of annual publications is lower than 2019. Plausibly, this may be attributed to the corona virus pandemic and its attendant lockdown and restrictions that may have prevented researchers from accessing their laboratories and pandemic-induced delays in the editorial review process. Cumulatively, 700 research articles are indexed in the Scopus database as of 14th August 2022. It is expected that this increase will continue in the following years as researchers design more developmental alloys and more application areas are explored.

## 3.2 Preferred journals for publishing PM-processed HEA/MCA

It is of utmost importance to identify the most preferred journals for publishing works on PM-processed HEA/MCA research. Researchers and funders can easily recognize

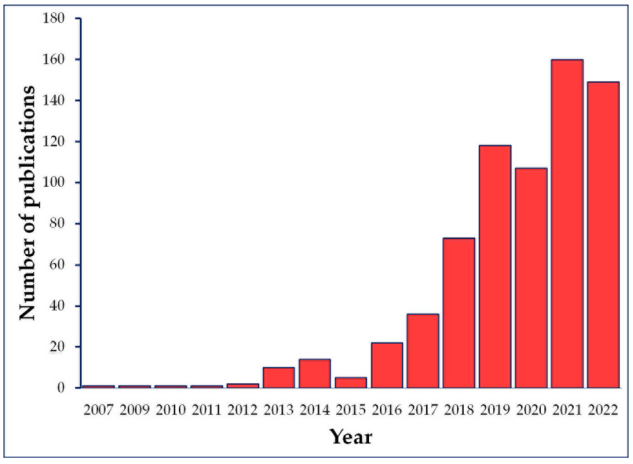


**Figure 2:** Annual scientific outputs on PM processing of HEA/MCA.

important up-to-date sources of information and key outlets for disseminating new ideas and gaining recognition for their efforts. High journal reputation has been shown to enhance article citation [55,56].

Figure 3 shows the article network map of the top 20 research journals for publishing PM-processed HEA/MCA works. The map is generated by setting the minimum number of articles in a journal and minimum number of citations of a journal to 5 and 20, respectively. It should be pointed out that the bibliometric literature does not contain standardized criteria for generating this type of network map [46]. However, we have chosen these criteria for easier analysis of the 142 unique scientific journals.

Consequently, 37 of these journals meet these criteria and are shown in Figure 3. A ranking of the top 20 journals based on the number of published articles, citations, and total link strength is shown in Table 1 below. The *total link strength* is an attribute that measures the total strength of the links of an item (*e.g.*, journal, author, *etc.*) with other items under analysis [57].

In Figure 3, there are five clusters of journals indicated in different colors. Cluster 1 (red; ten journals), cluster 2 (green; nine journals), cluster 3 (blue; five journals), cluster 4 (yellow; five journals), and cluster 5 (purple; four journals). Journals clustered in the same group have higher co-citation than journals in other clusters. Besides, the size of a node assigned to a journal indicates its influence based on the number of publications (or citations). In addition, the shorter the length of line between two journals, the stronger the relationship between them [53]. Therefore, the most preferred journal is the *Journal of Alloys and Compounds* with the highest *total link strength* (41), number of published articles (116), and citations (2,772). This journal publishes more than twice the number of articles in the next ranked journal, *i.e.*, *Materials Science and Engineering A* (50 articles, 1,641 citations). The next three are *Intermetallics, Materials Letter, and International Journal of Refractory Metals and Hard Materials*. Put together, these five journals have published a combined 34% of all PM-processed HEA/MCA works. Although these journals appear to be the most preferred outlets due to the number of publications, *Acta Materialia* has 1,276 citations from only 8 publications. This strongly indicates that the quality of research works in this journal is quite high. Other factors that may contribute to high citation counts include novelty, reputation of publishing journal, and journal publication model (open access or subscription-based) [55,56,58].

## 3.3 Scientific collaboration networks

### 3.3.1 Analysis of co-authorship of researchers

Scientific cooperation among researchers is important for enabling knowledge exchange and technology transfer,

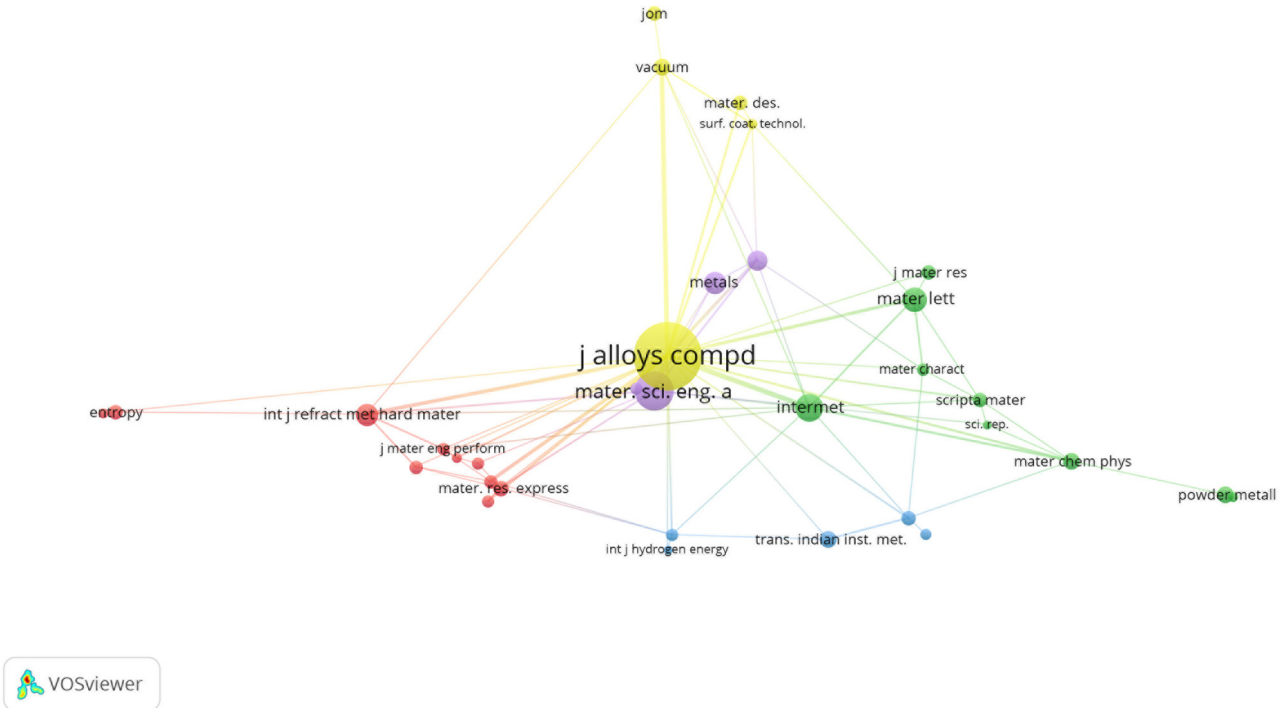


**Figure 3:** Network map of the top research journals for publishing PM-processed HEA/MCA.

**Table 1:** Bibliometric analysis of the top 20 research journals

| S. No. | Journal | Cluster | Number of articles | Citations | Links | Total link strength |
|---|---|---|---|---|---|---|
| 1 | Journal of Alloys and Compounds | 2 | 116 | 2,772 | 14 | 41 |
| 2 | Materials Science and Engineering A | 6 | 50 | 1,641 | 9 | 17 |
| 3 | Intermetallics | 1 | 29 | 682 | 11 | 20 |
| 4 | Materials Letters | 1 | 24 | 387 | 6 | 10 |
| 5 | International Journal of Refractory Metals and Hard Materials | 5 | 21 | 243 | 7 | 13 |
| 6 | Metals | 6 | 21 | 133 | 3 | 3 |
| 7 | Materials | 6 | 15 | 159 | 5 | 5 |
| 8 | Materials Chemistry and Physics | 1 | 14 | 224 | 6 | 8 |
| 9 | Powder Metallurgy | 1 | 13 | 49 | 2 | 2 |
| 10 | Transactions of the Indian Institute of Metals | 4 | 13 | 124 | 2 | 3 |
| 11 | Vacuum | 2 | 13 | 185 | 5 | 13 |
| 12 | Materials Research Express | 3 | 12 | 74 | 6 | 8 |
| 13 | Advanced Powder Technology | 4 | 11 | 208 | 6 | 7 |
| 14 | Entropy | 5 | 11 | 143 | 2 | 2 |
| 15 | JOM | 2 | 11 | 229 | 1 | 1 |
| 16 | Journal of Materials Research | 1 | 11 | 262 | 1 | 1 |
| 17 | Materials and Design | 2 | 11 | 644 | 2 | 4 |
| 18 | Scripta Materialia | 1 | 11 | 182 | 5 | 5 |
| 19 | Journal of Materials Science and Technology | 5 | 10 | 141 | 2 | 3 |
| 20 | Journal of Materials Engineering and Performance | 3 | 9 | 140 | 3 | 3 |

gaining access to expensive and specialized research facilities, and it is also an important indices for grading universities [45,51]. In VOSviewer, co-authorship cluster density map of authors is generated by using the criteria "minimum number of documents of an author = 5" and the "minimum number of citations of an author = 10." Figure 4 shows the cluster density map. One hundred and forty-one authors of the 1,961 researchers in the

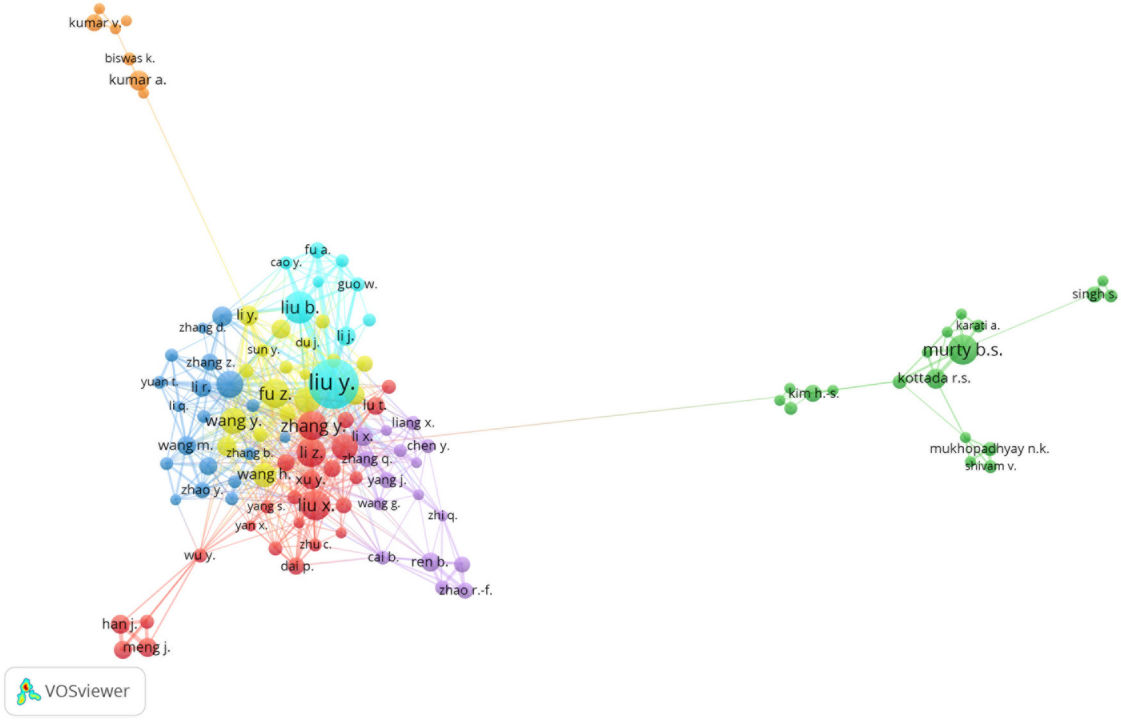


**Figure 4:** Co-authorship clustering map of authors based on number of publications.

database meet these criteria. However, only the top 113 connected researchers are shown in the co-authorship cluster density map in Figure 4, while the top 10 authors based on *total link strength* and other ranking attributes are shown in Table 2. From Figure 4, researchers are grouped into seven clusters represented by red (*Cluster 1*; 25 researchers), green (*Cluster 2;* 19 researchers), blue (*Cluster 3;* 19 researchers), yellow (*Cluster 4;* 18 researchers), purple (*Cluster 5;* 16 researchers), cyan (*Cluster 6;* 9 researchers), and orange (*Cluster 7;* 7 researchers). Scientists in each cluster represent a collaborating group. The brightness of a node associated with a researcher implies a stronger, collaborative network. Apparently, the most influential researchers in each of these clusters are Liu Y. (cyan; 48 articles; 45 collaborators), Murty B. S. (green; 22 articles; 7 collaborators), Zhang M. (blue; 18 articles; 24 collaborators), Fu Z. (yellow; 21 articles; 18 collaborators), Li X. (purple; 11 articles; 22 collaborators), Liu X. (red; 22 articles; 23 collaborators), and Kumar A. (brown; 12 articles; 3 collaborators. Of all these clusters, the overall most prominent author is Liu Y. He has research collaborators in all other clusters except the *green* and *brown* clusters. In most cases, his collaborators are the most prominent in their respective clusters. There are several factors that may affect the diversity of research collaboration. Some of these are the availability of a large number of foreign postgraduate students/visiting scholars and big research funds [51].

Table 2 presents more details about the collaborative network of the top 10 most prolific authors. The five most prolific authors are Liu Y. (48 articles), Liu B. (24 articles), Liu X. (22 articles), Murty B. S. (22 articles), and Fu Z. (21 articles). However, the positions of these authors change when they are ranked based on *citations*. Thus, the top five are Liu Y. (1,531 citations), Murty B. S. (1,296 citations), Kottada R. S. (1,124 citations), Liu B. (1,074 citations), and Fu Z. (934 citations). It is clear from this new list that many published articles by an author do not necessarily imply more citation counts. High citation counts are more likely to be associated with the quality of a research work, novelty, reputation of publishing journal, and access type (open access or subscription-based) [55,56].

### 3.3.2 Analyses of institutional and international co-authorship

Results in Table 3 show the analysis of institutional co-authorship. The criteria for generating the results include setting "minimum number of documents of an institution" and "minimum number of citations of an institution" to 5 and 10, respectively. Sixty-seven out of 964 institutions satisfy these conditions, but only the top ten institutions are indicated in Table 3. Furthermore, only 19 of these 67 institutions have collaborative links with the other institutions, suggesting that there is a low inter-institutional collaboration. The highest number of articles (31) and citations (1,509) are linked to the Indian Institute of Technology (IIT) Madras, India. This is followed closely, in terms of number of publications, by the Central South University (CSU), China. Although IIT has published ten more research articles than CSU, the citations count of IIT is more than 400% higher than that of CSU. It is highly likely that the articles from IIT are of higher quality and in highly reputed journals than those of CSU.

However, the *total link strengths* of all the institutes are relatively low. The *total link strength* is an attribute that indicates the strength of co-authorship of an item (*e.g.*, institutions) with others [57]. This implies that most of these institutions have reatively low collaboration with the other institutions. Likewise, of the ten institutions listed in Table 3, half are located in China based on the *total number of research articles*. To advance knowledge in this field, it is imperative to encourage and establish inter-institutional and international collaborations.

**Table 2:** Analysis of co-authorship of authors

| S. No. | Author | Cluster | Number of articles | Citations | Institution/country |
|---|---|---|---|---|---|
| 1 | Liu Y. | 2 | 48 | 1,531 | Sichuan University, Chengdu, China |
| 2 | Liu B. | 2 | 24 | 1,074 | Central South University, Changsha, China |
| 3 | Liu X. | 3 | 22 | 314 | Southwest Jiaotong University, Chengdu, China |
| 4 | Murty B.S. | 1 | 22 | 1,296 | Indian Institute of Technology Madras, Chennai, India |
| 5 | Fu Z. | 4 | 21 | 934 | Wuhan University of Technology, Wuhan, China |
| 6 | Zhang Y. | 3 | 21 | 319 | Nanjing Institute of Technology, Nanjing, China |
| 7 | Li Z. | 3 | 20 | 286 | Chinese Academy of Sciences, Hefei, China |
| 8 | Zhang M. | 5 | 18 | 181 | Central South University, Changsha, China |
| 9 | Chen J. | 3 | 17 | 255 | Xi'an Technological University, Xi'an, China |
| 10 | Chen W. | 3 | 17 | 500 | South China University of Technology, Guangdong, China |

**Table 3:** Analyses of institutional co-authorship

| S. No. | Institution | Country | Number of published articles | Links | Total link strength | Citations |
|---|---|---|---|---|---|---|
| 1 | Indian Institute of Technology Madras (Department of Metallurgical and Materials Engineering), Chennai | India | 31 | 5 | 15 | 1,509 |
| 2 | Central South University (State Key Laboratory of Powder Metallurgy), Changsha | China | 21 | 7 | 10 | 362 |
| 3 | Chinese Academy of Sciences (State Key Laboratory of Solid Lubrication, Lanzhou Institute of Chemical Physics), Lanzhou | China | 18 | 2 | 7 | 434 |
| 4 | Zhengzhou University (School of Physics and Engineering), Zhengzhou | China | 13 | 2 | 8 | 161 |
| 5 | Ajou University (Department of Materials Science and Engineering), Suwon | South Korea | 12 | 2 | 11 | 52 |
| 6 | Russian Academy of Sciences (Merzhanov Institute of Structural Macrokinetics and Materials Science), Chernogolovka | Russian Federation | 12 | 2 | 7 | 60 |
| 7 | Yuanmeng Precision Technology (Shenzhen) Institute, Shenzhen | China | 10 | 6 | 17 | 151 |
| 8 | Nanjing Agricultural University (College of Engineering), Nanjing | China | 9 | 3 | 10 | 52 |
| 9 | Ajou University (Department of Energy Systems Research), Suwon | South Korea | 9 | 1 | 9 | 50 |
| 10 | Pohang University of Science and Technology (Department of Materials Science and Engineering), Pohang | South Korea | 9 | 2 | 6 | 88 |

Other than inter-institutional collaboration, international research collaborations are equally important means of enhancing knowledge sharing and technology transfer. Figure 5 shows the density map of the countries with the highest number of publications. To generate this figure in VOSviewer, the "minimum number of documents of a country" is set to 5 while the "minimum number of citations of a country" is set to 10. All PM-based HEA/MCA articles are affiliated with 58 countries according to the data retrieved from the Scopus database but only 31 meet this threshold, as shown in Figure 5. However, two countries – Egypt (*Links* 1, *Research articles* 9*; Citations* 36) and South Africa (*Links* 0, *Research articles* 7*; Citations* 37) – are excluded from the map due to not having significant number of co-authorships with other nations. The brightest and largest spot is linked to China (299 articles), followed by India (115 articles), and then South Korea (56 articles). The brightness of a spot indicates the density (or number) of articles published by the country associated with the node.

All the countries are connected showing that international collaboration is well established. A summary of the statistics of the top ten most prolific countries is presented in Table 4.

The highest number of publications (299) and citation counts (5,634) emanates from China. In fact, Chinese publications in the period under review exceed the sum of publications from the next top four countries, *i.e.*, India, South Korea, United States, and Germany.

## 3.4 Citations analysis of most influential articles on PM-processed HEA/MCA

Figure 6 below shows the citations analysis of the most influential articles on PM-processed HEA/MCA. This section presents the results of the analysis of the most influential publications. The minimum number of citations of a document is selected to be 20 with 195 of the 700 articles meeting this criterion. However, only the top 50 are shown in Figure 6. Despite that the first articles in this field appear pre-2010 [37,59,60], the top five most cited are published post-2011 [61–65]. This is a bit strange; pioneering research articles usually have the highest citation counts as newer articles continue to refer to them. In the broad field of HEA/MCA, the most cited articles are those of Yeh *et al.* [2] and Cantor *et al.* [1], the pioneering publications on HEA/MCA. These two articles have more than 6,800 citations between them.

In the sub-field of PM-processed HEA/MCA, the most influential article in terms of citation count is Liu *et al.* [61] with 456 citations, Followed by Senkov *et al.* [62] with 420

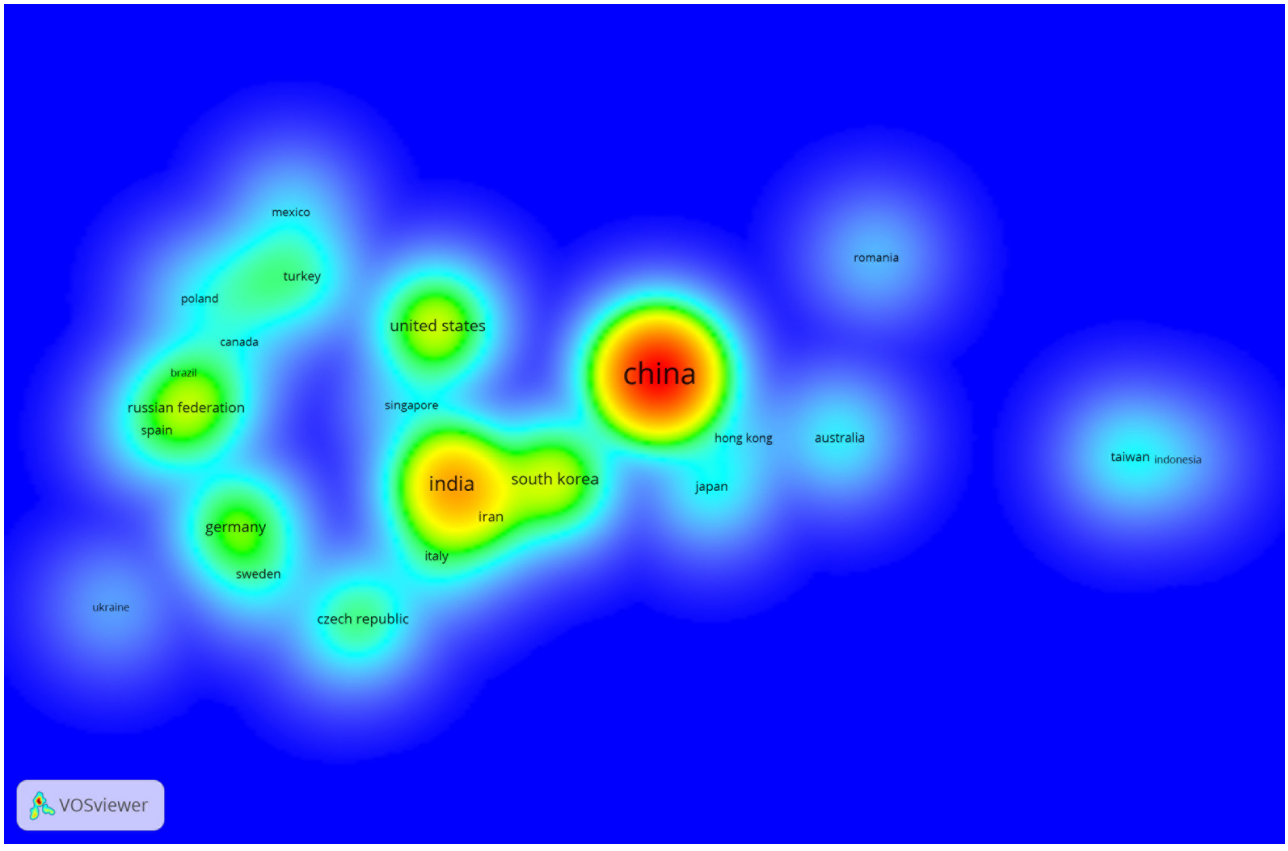


**Figure 5:** Density map of co-authorship of countries measured by number of scientific publications.

**Table 4:** Top ten most prolific countries in the field of PM-processed HEA/MCA

| S. No. | Country | Number of articles | Citations |
|---|---|---|---|
| 1 | China | 299 | 5,634 |
| 2 | India | 115 | 2,641 |
| 3 | South Korea | 56 | 765 |
| 4 | United States | 56 | 2,777 |
| 5 | Germany | 39 | 862 |
| 6 | Russian Federation | 24 | 201 |
| 7 | Czech Republic | 23 | 402 |
| 8 | France | 22 | 324 |
| 9 | Iran | 22 | 108 |
| 10 | Turkey | 17 | 171 |

citations and Youssef *et al.* [63] with 368 citations. Completing the top five most cited articles are Praveen *et al.* [64] (274 citations) and Senkov *et al.* (272 citations) [65]. More details about these most-cited articles and publication outlets are contained in Table 5.

## 3.5 Co-occurrence network of author keywords

A co-occurrence network is useful for recognizing important research areas and potential future research directions [46]. In VOSviewer, the co-occurrence network map of author keywords is generated by setting the minimum number of occurrences of a keyword at 5. In all, there are 684 keywords of which 86 meet this threshold. Each circular node in Figure 7 represents a keyword, while the size of a node is proportional to the number of articles in which the keyword occurs. The distance between any two keywords is a measure of their relatedness. This implies that related keywords have shorter distance between them. Finally, a group of keywords may have the same color and therefore, belong to the same cluster. This implies that such keywords in the same cluster tend to co-occur together more than keywords in a different cluster [48].

All the 86 keywords are grouped into seven clusters. The cluster with largest number of keywords (*i.e.*, 18) is

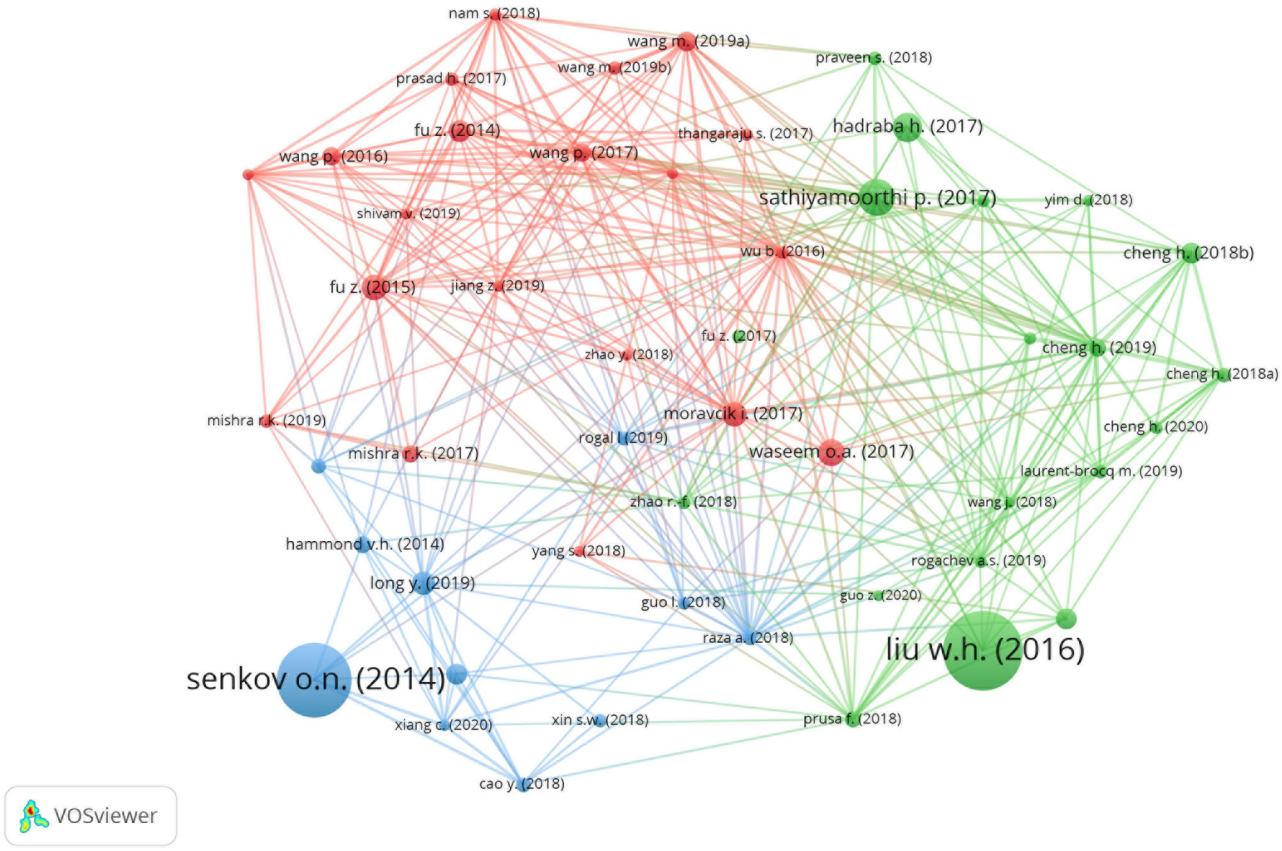


**Figure 6:** Network map of most-cited PM-processed HEA/MCA research articles.

*cluster 1* in red and has "high entropy alloy" as the most prominent (492 occurrences and 85 links with other keywords). Some of the other keywords in the same cluster are *HEA composites, laser sintering, compressive properties, microwave sintering, intermetallic compounds, deformation behavior, plastic deformation, etc*. *Cluster 2* is in *green* with 18 keywords. The most frequently occurring here is *mechanical alloying* (210 occurrences, with 70 links). This indicates that the preferred production method is by mechanical alloying, rather than powder mixing or additive manufacturing, for instance. Other co-occurring keywords in the same cluster with "mechanical alloying" are *phase evolution, annealing, nanocrystalline HEAs, process control agents, oxide dispersion strengthening, molecular dynamics, etc*. All these keywords have strong correlation with "mechanical alloying." For instance, mechanical alloying is a prominent method to obtain nanocrystalline structure, which often requires the use of "process control agents" to minimize cold welding.

*Cluster 3* appears in *blue* and contains a group of 13 keywords. Some of these include *vacuum hot pressing* (5 occurrences, 11 links), *powder metallurgy* (128 occurrences, 60 links), *HEA carbides* (6 occurrences, 12 links), *HEA ceramics* (6 occurrences, 10 links), *friction and wear behavior* (129 occurrences, 84 links), *etc*. The yellow cluster is *Cluster 4* with 13 keywords including *corrosion behavior, HEA coatings, heat treatment, magnetron sputtering, etc*. Of all these *Cluster 4* keywords, the most frequently used is *corrosion behavior* with 40 mentions and 37 links. *Clusters* 5 (9 keywords), 6 (8 keywords), and 7 (6 keywords) are coded purple, cyan, and brown, respectively.

Going by the number of articles retrieved from the Scopus database, PM-processing of HEA/MCA is still evolving. Therefore, other than the conventional "sintering" techniques, others like "spark plasma sintering," "microwave sintering," and "vacuum hot pressing" have been investigated in the literature. Among the different consolidation techniques, the most preferred is the *SPS* (142 mentions, 63 links). This may not be unconnected to its unique advantages including rapid sintering in a matter of minutes, lower sintering temperature, which is beneficial for minimizing phase transformation, and its ability to maintain the nanocrystalline structure obtained from the high-energy/mechanical milling process [25,26]. As indicated by its high occurrence, this method has been well researched in the literature.

**Table 5:** Top 20 most-influential PM-processed HEA/MCA articles

| S. No. | First author and year | Article title | Journal | Citations |
|---|---|---|---|---|
| 1 | Liu W. H. [61] | Ductile CoCrFeNiMox high entropy alloys strengthened by hard intermetallic phases | Acta Materiala | 456 |
| 2 | Senkov O. N. [154] | Effect of aluminum on the microstructure and properties of two refractory high-entropy alloys | Acta Materiala | 420 |
| 3 | Youssef K. M. [63] | A novel low-density, high-hardness, high-entropy alloy with close-packed single-phase nanocrystalline structures | Materials Research Letters | 368 |
| 4 | Praveen S. [64] | Alloying behavior in multi-component AlCoCrCuFe and NiCoCrCuFe high entropy alloys | Materials Science and Engineering A | 274 |
| 5 | Senkov O. N. [65] | Microstructure and properties of a refractory NbCrMo0.5Ta0.5TiZr alloy | Materials Science and Engineering A | 272 |
| 6 | Ji W. [28] | Alloying behavior and novel properties of CoCrFeNiMn high-entropy alloy fabricated by mechanical alloying and spark plasma sintering | Intermetallics | 214 |
| 7 | Ji W. [155] | Mechanical alloying synthesis and spark plasma sintering consolidation of CoCrFeNiAl high-entropy alloy | Journal of Alloys and Compounds | 175 |
| 8 | Chen Y.-L. [60] | Competition between elements during mechanical alloying in an octonary multi-principal-element alloy system | Journal of Alloys and Compounds | 155 |
| 9 | Sriharitha R. [156] | Alloying, thermal stability, and strengthening in spark plasma sintered $Al_xCoCrCuFeNi$ high entropy alloys | Journal of Alloys and Compounds | 152 |
| 10 | Praveen S. [157] | Exceptional resistance to grain growth in nanocrystalline CoCrFeNi high entropy alloy at high homologous temperatures | Journal of Alloys and Compounds | 125 |
| 11 | Pradeep K. G. [158] | Atomic-scale compositional characterization of a nanocrystalline AlCrCuFeNiZn high-entropy alloy using atom probe tomography | Acta Materialia | 116 |
| 12 | Sriharitha R. [159] | Phase formation in mechanically alloyed $Al_xCoCrCuFeNi$ ($x$ = 0.45, 1, 2.5, 5 mol) high entropy alloys | Intermetallics | 111 |
| 13 | Ang A. S. M. [160] | Plasma-sprayed high entropy alloys: microstructure and properties of AlCoCrFeNi and MnCoCrFeNi | Metallurgical and Materials Transactions A | 110 |
| 14 | Hsu U. S. [59] | Alloying behavior of iron, gold, and silver in AlCoCrCuNi-based equimolar high-entropy alloys | Materials Science and Engineering A | 107 |
| 15 | Varalakshmi S. [37] | Hot consolidation and mechanical properties of nanocrystalline equiatomic AlFeTiCrZnCu high entropy alloy after mechanical alloying | Journal of Materials Science | 103 |
| 16 | Praveen S. [26] | Phase evolution and densification behavior of nanocrystalline multicomponent high entropy alloys during spark plasma sintering | JOM | 91 |
| 17 | Zhang A. [161] | Rapid preparation of AlCoCrFeNi high entropy alloy by spark plasma sintering from elemental powder mixture | Materials Letters | 81 |
| 18 | Fu Z. [162] | Effects of Co and sintering method on microstructure and mechanical behavior of a high-entropy Al0.6NiFeCrCo alloy prepared by powder metallurgy | Journal of Alloys and Compounds | 80 |
| 19 | Yu P. F. [163] | Effects of high-pressure torsion on microstructures and properties of an Al0.1CoCrFeNi high-entropy alloy | Materials Science and Engineering A | 79 |
| 20 | Wang B. [164] | Mechanical properties and microstructure of the CoCrFeNiMn high entropy alloy under high strain rate compression | Journal of Materials Engineering and Performance | 68 |

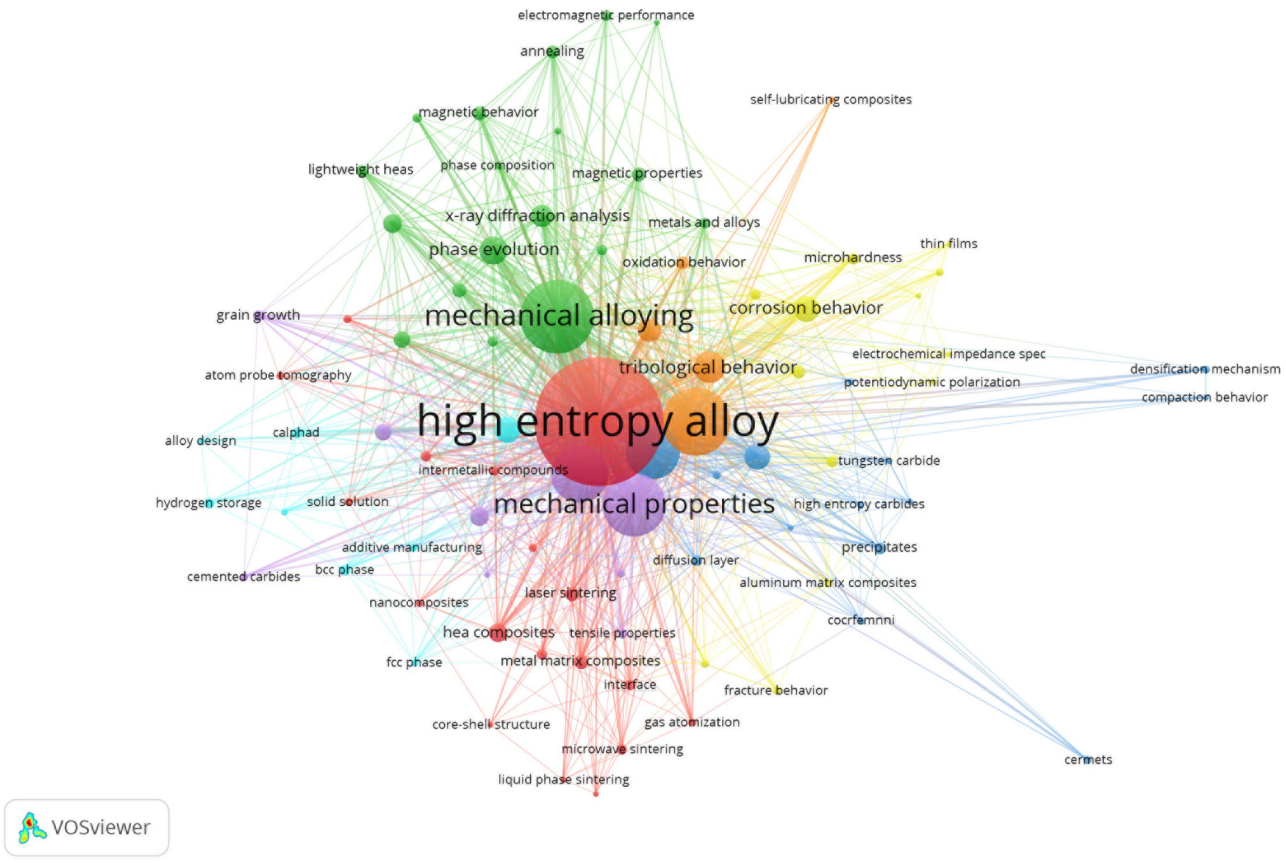


**Figure 7:** Co-occurrence network map of author keywords.

Other than this consolidation technique, there are also a few reports on using the *microwave sintering* technique (14 occurrences). One of the first works using this approach is reported by Veronesi and co-workers [36]. Given that it is a very rapid sintering process (*e.g.*, 180 s of sintering time [36]), this technique offers similar advantages associated with SPS. Therefore, it has been widely used to consolidate various traditional metal matrix composites (MMCs) [66–68]. Nonetheless, it may be of scientific interest to compare the properties of HEA/MCA materials consolidated *via* SPS technique with the microwave sintering technique.

Majority of the studies on PM-processed HEA/MCA have focused on investigating mechanical properties. This explains the relatively high occurrences (keyword variants include *compressive behavior, microhardness, tensile, mechanical testing*, *etc.*) in the literature. Nonetheless, other functional properties such as *tribological properties* (56 occurrences), *electrochemical impedance* (five occurrences), *electromagnetic* (two occurrences), *magnetic* (17 occurrences), *thermo-electric* (14 occurrences), and *thermal analysis* (14 occurrences) have also been investigated. However, the low number of occurrences for electrochemical, thermoelectric, and electromagnetic indicates that future research directions may consider these properties for investigation and application areas.

Departing from the traditional applications (*e.g.*, refractory materials, hard materials, *etc.*), some functional applications of PM-processed HEA/MCA have also appeared in the literature. This explains why keywords like *hydrogen storage* and *electromagnetic properties*, have been investigated. However, all these keywords have been used less than ten times in the examined literature. More future research works may be needed in these directions to fully harness the potentials offered by HEA/MCA for these applications.

The bulk of the works retrieved are biased towards laboratory experiments. To predict stable phases and their relative amounts, reduce cost, and minimize developmental time of important alloys, machine learning/computational approaches may be adopted [69,70]. In traditional PM processing, machine learning approach has been successfully deployed to predict the particle sizes of mechanically-milled magnesium-based metal powder [71] and discover novel nickel superalloys [72]. To this end, “calphad” (CALculation of PHAse Diagrams) has been used in the PM-based HEA/MCA literature about seven times. Some of these works are in the cited references [73,74]. In the broad field of HEA/

MCA, it is encouraging that some recent works have adopted this approach [70,75,76]. To fully harness the potentials of this computational approach, more future research efforts may be devoted to this niche.

One of the core strengths of PM-processing is its versatility in producing difficult-to-melt and refractory alloys. For this, a keyword like *refractory high entropy alloy* has been used about 41 times in the surveyed literature on PM-HEA/MCA. Other associated keywords with similar use are *cermets, cemented carbides, wear*, and *oxidation behavior*. It is equally important to note that some keywords have been excluded from analysis due to not meeting the minimum of 5 occurrences threshold. Some of these include keywords associated with physical properties (*e.g.*, dielectric properties, machinability – one occurrence each), processing techniques (*e.g.*, severe plastic deformation, hot forging, metallothermic reduction, self-propagating high-temperature synthesis – one occurrence each), theoretical modeling (*e.g.*, density functional theory, thermo-calc *etc.*). The occurrence of these keywords less than five times is an indication that they are potential future research directions.

### 3.6 Limitations of bibliometric study

One of the limitations of the bibliometric analyses in this study is that we have limited literature retrieval to a single database (*i.e.*, Scopus). It is likely that some important articles may have not been indexed in this database. Future works may consider combining articles from several databases. Furthermore, our data exclude articles not published in English language. Finally, other academic sources, such as conferences, books, encyclopedia, *etc.*, have not been considered in our analysis.

## 4 Review of deformation studies and some selected functional application areas

Recently, some reviews regarding PM-HEAs were published [38,77–79]. The authors analyzed the PM consolidation techniques, mechanical properties, and compared the alloying elements used in developing PM-HEAs with the as-cast HEAs. For example, Torralba *et al.* [38] reviewed production techniques and functional properties of PM-HEA articles published between 2008 and 2018. Their work covered high-temperature mechanical, corrosion and oxidation, magnetic properties, hydrogen storage, MMCs and oxide dispersion strengthened alloys. However, some functional areas are detected in this study by co-occurrence network of author keywords, which have not been reported in earlier studies or reported but new findings have emerged which are worth assessing.

Therefore, new findings of some functional applications in PM-HEAs from 2019 to 2022 are discussed in Section 4. These include deformation of PM-HEAs (negative strain rate sensitivity [SRS], equiaxed grains microstructure, and grain boundary bulging); thermoelectric properties (composition tuning and addition of dopants such as bismuth (Bi) and gallium (Ga) in multi-component thermoelectric alloys); tribological properties ($TiB_2$, $Cr_3C_2$, and $ZrO_2$ composites for wear resistance); oxidation (oxidation properties of cantor alloys containing a Y-Ti-O particle and spallation occurrence); corrosion (coumarin as an inhibitor for Mg HEAs, carbon nanotubes for corrosion resistance in HEAs); hydrogen storage (hydrogen storage properties in lightweight Mg HEAs), and radiation (grain growth rate, self-healing mechanism, higher surface stability under irradiation fluence).

### 4.1 Tribological application

PM techniques have provided opportunities to develop a reliable and efficient production of advanced materials, such as HEAs [80]. The process is well suited for producing fine-grained homogenous microstructures and wear resistant materials from HEA-based composites [81]. Hard ceramic particles provide a wide range of improved mechanical properties, such as hardness, wear resistance, and compressive strength when combined with MMCs [82,83]. An FCC phase and a $Cr_7C_3$ phase were formed during the sintering of CoCrFeNiMn HEA after the addition of $Cr_3C_2$ to improve the tribological properties of the material [84]. When CoCrFeNiMn HEA was prepared without the addition of $Cr_3C_2$ particles, the Vickers hardness was 181.2 HV, whereas increasing the amount of $Cr_3C_2$ by 10, 20, and 40% increased the hardness to 323.2, 417.0, and 681.6 HV, respectively. Figure 8 depicts the friction coefficients of CoCrFeNiMn and CoCrFeNiMn-$Cr_3C_2$ at various temperatures under different conditions. According to Figure 8a, the friction coefficient of the CoCrFeNiMn HEA was 0.62 at room temperature, and it further decreased as the temperature rose to 200, 400, 600, and 800°C.

This decrease in friction coefficient was primarily due to the oxide lubrication and matrix softening effects at higher temperatures. With the increase in the $Cr_3C_2$ content (Figure 8a), the friction coefficient decreased until it

reached 20%, after which it increased until it reached 40%. As a result, CoCrFeNiMn HEA matrix composites exhibited excellent ability to reduce friction. CoCrFeNiMn HEA wear rate (Figure 8b) decreased with the increase in the temperature, from $5.60 \times 10^{-4}$ $mm^3 \cdot Nm^{-1}$ at room temperature to $7.17 \times 10^{-6}$ $mm^3 \cdot Nm^{-1}$ at 800°C. When the content of $Cr_3C_2$ in CoCrNiMn HEA was increased by 10, 20, and 40%, the wear rate at room temperature decreased from $5.60 \times 10^{-4}$ $mm^3 \cdot Nm^{-1}$ to $0.98 \times 10^{-5}$ $mm^3 \cdot Nm^{-1}$, and $0.56 \times 10^{-5}$ $mm^3 \cdot Nm^{-1}$. This was primarily due to the improvement in hardness [84]. The wear rates of CoCrFeNiMn HEA, CoCrFeNiMn-10% $Cr_3C_2$ composite, and CoCrFeNiMn-40% $Cr_3C_2$ composite all remained constant at 800°C, but the wear rate of CoCrFeNiMn-20% $Cr_3C_2$ composite was significantly higher. In general, the CoCrFeNiMn-10% $Cr_3C_2$ composite exhibited excellent wear resistance from room temperature to 800°C.

Using AlCoCrFeNi–$ZrO_2$ HEA composites, Ghanbariha *et al.* [85] investigated the effect of $ZrO_2$ particles on the nanomechanical properties and wear behavior. The AlCoCrFeNi–$ZrO_2$ composite was synthesized using a mechanical alloying process combined with SPS at 1,000°C. The sintered samples comprised two main phases: FCC and BCC, and minor phases: Al-rich and Cr-rich. This was due to the short duration of the SPS process, which did not allow for the conversion of the non-equilibrium BCC phase into the equilibrium FCC phase [85]. As a result, a combination of FCC and BCC phases were found. For the effect of zirconia content on the wear resistance of AlCoCrFeNi–$ZrO_2$, it was discovered that zirconia reinforcement content from 0 to 5 wt% only slightly improved the wear resistance due to a balance of positive effects of $ZrO_2$ particle addition and negative effects of BCC phase reduction. When there was an increase in zirconia particles to 10 wt%, the elastic to strain ratio (H/E) of the FCC phase remained constant, while the H/E ratio of the BCC phase moderately increased. Despite the H/E effect, it appeared that the positive effect of the addition of 10 wt% zirconia played a more significant role in the improvement of wear resistance. According to the wear width analysis, the pure HEA sample had the largest wear width (1932.58 μm), followed by the 5% $ZrO_2$ sample (1825.84 μm), and the smallest wear width was found in the 10 wt% zirconia particles sample (1433.20 μm). Consequently, the AlCoCrFeNi-10 wt% $ZrO_2$ sample exhibited the best wear performance of the three samples tested.

Kang *et al.* [81] investigated the effect of $TiB_2$ on the tribological properties of AlCoCrFeNi using ball milling and SPS at 1,200°C, and detected the following phases: B2, BCC, FCC, and $TiB_2$. The microstructure consisted of spherical or near-spherical particles, which become more pronounced with increased $TiB_2$ content, indicating that $TiB_2$ could inhibit the bonding of the AlCoCrFeNi powders during the sintering process. Furthermore, when the $TiB_2$ content of the AlCoCrFeNi particles was increased, a significant agglomeration phenomenon was observed between the AlCoCrFeNi particles. It was discovered that increasing the $TiB_2$ content in AlCoCrFeNi/$TiB_2$ composites caused an increase in the amount of boron oxide present in the tribological film, which resulted in a decrease in the values of coefficient of friction (COF). When the $TiB_2$ content increased from 0 to 30%, the wear rate of the composites decreased from $5.84 \times 10^{-4}$ to $0.93 \times 10^{-4}$ $mm^3 \cdot m^{-1}$, indicating a decrease in the wear rate of the composite. It was also reported in additive manufactured CoCrFeMnNi/$TiB_2$ composites that wear rate decreased from 3.42 to 1.48 $mm^3 \cdot Nm^{-1}$

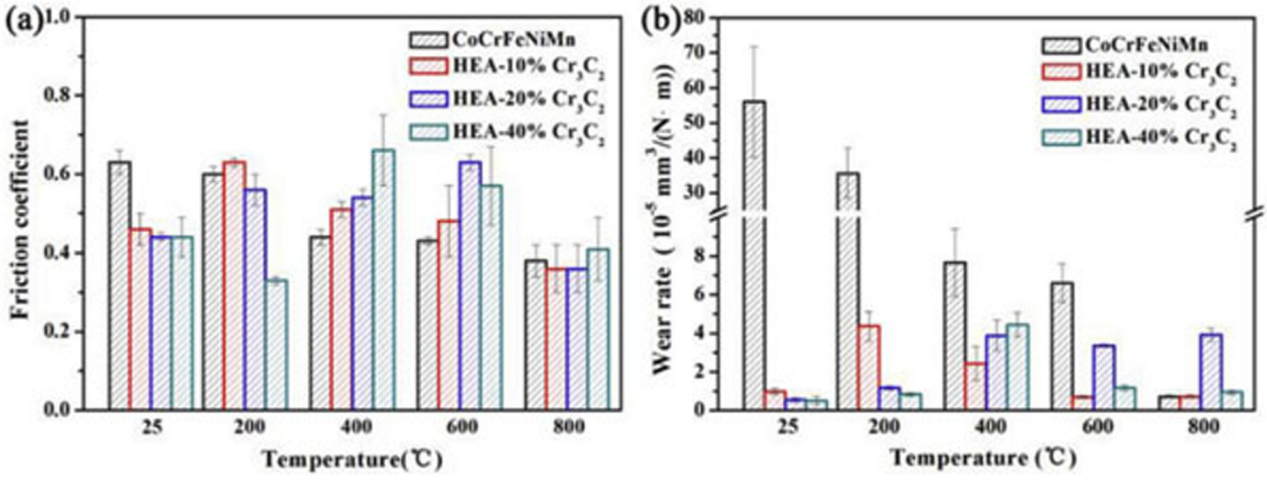


**Figure 8:** (a) Friction coefficients and (b) wear rates of CoCrFeNiMn HEA and its composites at RT, 200, 400, 600, and 800°C. Reproduced with permission [84]. Copyright 2021, Elsevier.

due to $TiB_2$ addition [86]. This clearly demonstrates that increasing the $TiB_2$ content in AlCoCrFeNi/$TiB_2$ composites increases the wear resistance. Additionally, the boron oxide formed during the tribological oxidation of $TiB_2$ played a significant role in the formation of solid lubricants.

Wang *et al.* [86] studied the *in situ* formed graphene which provided lubricity for the FeCoCrNiAl-graphene (FeCoCrNiAl-G) based composite. The COF of FeCoCrNiAl increased with the increase in the force and frequency at 5 N and 1 Hz, respectively, and remained stable at a high value. However, when the load was greater than 20 N and the velocity was greater than 3 Hz, the COF showed a decreasing trend in the running period. This was especially noticeable when the load was greater than 40 N and the frequency was greater than 6 Hz [86]. When the HEA-G was operated at a load less than 30 N, the COF decreased initially from 0.2 to approximately 0.16 in the steady state; when the load was greater than 40 N, the COF was also reduced to a steady state after the initial 300 cycles. The study revealed that the original FeCoCrNiAl HEA had poor tribological properties when subjected to low loads and velocities. The addition of graphite nanoplate improved the tribological properties of the original HEA significantly under low loads and velocities, with a reduction in COF of 80% at a load of 5 N (0.15 *vs* 0.84) and a reduction in wear of nearly two orders of magnitude. The sliding and shearing produced by graphene were primarily responsible for the dramatic reduction in friction and wear (below ten layers). Another way that the tribo-chemical reaction improved tribological properties was by forming a tribo-layer that had metallic and partially oxidized metal oxide nanoparticles in it, which could also help improve the tribological properties. Similarly, tribological properties improvement through tribo-layer containing oxidized metal oxide was reported in graphite-reinforced FeNiCrCuMo high-entropy alloy [87].

## 4.2 Oxidation resistance

HEAs are potentially applicable in high-temperature applications because of their exceptional oxidation resistance [88,89]. According to Butler and Weaver [89], the good oxidation resistance of HEA is because they are less compositionally constrained than conventional structural alloys and accommodate higher concentrations of the elements that are necessary to form protective external oxide scales such as Al or Cr. In addition, HEAs exhibit sluggish diffusion kinetics that could enhance their oxidation behaviors by inhibiting the formation of non-protective transient oxides [90]. Vilémová *et al.* [91] investigated the oxidation properties of CoCrFeMnNi and FeCoCrNi HEA alloys containing a Y-Ti-O particle produced by MA+SPS for 1–150 h at temperatures ranging from 750 to 950°C. The oxidation performance of the CoCrFeMnNi exhibited a two-stage oxidation behavior at 750°C. The oxidation rate in the second stage did not decrease with the thickness of the oxide layer; therefore, the alloy did not function as an effective oxidation barrier. However, after 150 h at 750°C, no significant oxide spallation was observed. It was discovered that removing Mn from the alloy composition significantly reduced the weight gain of FeCoCrNi and that the oxide served as a protective barrier against further oxidation after 150 h at 750°C. When heated to 950°C for 5 h, CoCrFeMnNi exhibited significant spallation. The spallation phenomenon was also observed in as-cast HEAs such as: $Fe_{22.63}Ni_{26.06}Co_{26.82}Mn_{24.47}$ at 750°C for 100 h [92]; AlCoCrFeNi at 10–30 h [89]; $Al_{0.9}$FeCrCoNi [93]; and $Al_{0.25}$CoCrCuFeNiMn at 700 and 900°C [94]. Spallation was attributed to high thermal stresses that developed within the substrate and the oxide layer during the cooling part of the exposure [93,94]. Similarly, Vilémová *et al.* [91] discovered that removing Mn from the FeCoCrNi alloy composition resulted in an improved protection of the alloy even at 950°C after 5 h.

The role of Al content on the cyclic oxidation of resistance of sintered CoCrFeNi$Al_x$ ($x$ = 0.7, 0.85, and 1 mol) was investigated in another study at 800, 875, and 950°C for 120 h [95]. Because of the higher Al content in CoCrFeNi$Al_1$, the parabolic rate constant (Kp) of CoCrFeNi$Al_1$ was lower than that of CoCrFeNi$Al_{0.7}$ and CoCrFeNi$Al_{0.85}$. The oxidation kinetics were similar to that reported in as-cast $Ni_2$FeCoCr$Al_x$ alloy during dry air-oxidation at $T \geq 700$°C [96]. This suggests that the addition of Al enhances the oxidation resistance of CoCrFeNi$Al_x$ HEAs. An increase in Al content also resulted in better oxidation resistances for arc melted AlCoCrFeNi HEA [89]. Furthermore, the Kp values increase as the oxidation temperature is raised, but they decrease as the Al content is raised. The CoCrFeNi$Al_1$ Kp value (0.01985 $mg^2 \cdot cm^{-4} \cdot h^{-1}$) increased slightly when heated to 800°C to 0.02954 $mg^2 \cdot cm^{-4} \cdot h^{-1}$ for the CoCrFeNi$Al_{0.7}$ alloy and further to 0.1399 $mg^2 \cdot cm^{-4} \cdot h^{-1}$ for the CoCrFeNi$Al_{0.85}$ alloy. The oxidation results obtained at 950°C for 120 h revealed an outer layer composed of $Cr_2O_3$ and an inner discontinuous layer ($Al_2O_3$) formed on the HEAs CoCrFeNi$Al_{0.7}$ and CoCrFeNi$Al_{0.85}$. This outer layer ($Cr_2O_3$) and inner discontinuous layer ($Al_2O_3$) were found in as-cast AlCoCrFeNi HEA oxidized at 1,050°C for 100 h [89] and as-cast AlCoCrFeNi oxidized at 1,000°C for 48 h [97]. The oxide scale of CoCrFeNi$A_1$ contained significantly more $Al_2O_3$ than CoCrFeNi$Al_{0.7}$ and CoCrFeNi$Al_{0.85}$. The increase in Al concentration led to an increase in the continuity of the $Al_2O_3$ subscale [89].

Zhang *et al.* [98] also varied Al content in spark plasma sintered $Al_xCrTiMo$ ($x$ = 0.25, 0.5, 0.75, 1) refractory HEAs. During the process of oxygen corrosion, the oxidation kinetics resulted in a moderate mass gain in the $Al_{0.5}CrTiMo$, $Al_{0.75}CrTiMo$, and AlCrTiMo refractory HEAs. However, there was a reduction in the rate of mass increase that occurred twice during the oxidation process of $Al_{0.25}CrTiMo$. This occurred because of the absence of protective alumina oxide layers forming on the surface of low Al-containing samples, or it could be attributed to a few spallation and delamination that occurred on the surface of low Al-containing samples. The oxidation layers, which extended from the exterior to the interior of the alloys, were composed of $TiO_2$, $Al_2O_3$, and $Cr_2O_3$. The findings of the study confirmed the importance of Al content in the oxidation resistance of HEAs.

## 4.3 Corrosion resistance

HEAs are being considered for potential corrosion-resistant applications because most elements in HEAs are corrosion-resistant and passivating. They are usually free of common corrosion initiating sites, such as impurities and inclusions [99]. The PM-HEAs have exhibited considerable compositional precision, especially the minimization of elemental segregation, which has been reported to improve the corrosion resistance of HEAs. For example, reported as-cast $Cu_{45}Mn_{25}Al_{15}Fe_5Cr_5Ni_5$ [100] and CuCrFeNiMn [101] HEAs showed decreased corrosion resistance due to elemental segregation. Zhou *et al.* [102] investigated the effect of annealing temperature on the corrosion properties of SPS-ed AlCoCrFeNi HEA in 0.5 mol·$L^{-1}$ $H_2SO_4$. In SPS-ed AlCoCrFeNi, B2, BCC, and FCC phases were discovered. During the annealing process at temperatures of 700, 800, and 900°C, the SPS-ed AlCoCrFeNi transformed to B2 + BCC + FCC + sigma. It was found that the corrosion potential and current density increased, and the polarization resistance decreased with the increase in the annealing temperature. The AlCoCrFeNi alloy annealed at 900°C showed the highest corrosion potential (0.315 V), current density (108 μA·$cm^{-2}$), and polarization resistance (401.2 Ω). The formed sigma phase during the annealing process decreased the corrosion resistance of the AlCoCrFeNi alloy. The sigma phase also dominated the corrosion process of as-cast $CoCrFeNiMo_{0.3}$ [103], with the corrosion resistance decreasing rapidly due to the sigma phase precipitation. In an as-cast CoCrFeMnNi HEAs [104], the sigma phase formed in the ultra-fine grain alloy after the annealing process resulted in galvanic corrosion between the sigma phase and its neighboring matrix phase.

Parakh *et al.* [105] investigated the crystal structure and grain size effects on the corrosion properties of SPS-ed AlNiCoCrFe, FeCrNiAlCo, CoNiFeCrAl, and as-cast AlCoCrFeNi HEAs in 3.5 wt% NaCl solution. The SPS-ed AlNiCoCrFe, FeCrNiAlCo, and CoNiFeCrAl alloys contained BCC and FCC phases. It was found that there was an improvement in corrosion resistance of FeCrNiAlCo and CoNiFeCrAl HEAs when the FCC content was 38 and 16%. For the AlNiCoCrFe alloy, an increase in FCC content to 62% led to a drop in corrosion resistance. Amongst the SPS-ed alloys, FeCrNiAlCo with an optimum FCC content of 38% had the best corrosion resistance. This is equivalent to the as-cast AlCoCrFeNi alloy. It was found that the as-cast AlCoCrFeNi alloy had better corrosion resistance than the SPS-ed alloys because the grains were bigger. It was also confirmed in as-cast CoCrFeMnNi HEAs where the coarse grained (48 μm) sample exhibited a better corrosion resistance than the ultra-fine-grained (0.689 μm) in 3.5 wt% NaCl solution [104]. The authors concluded that the corrosion resistance of an alloy was affected by three things: phase fraction, grain size, and dislocation density. Of these three, phase fraction is the most significant, while dislocation density is the least.

Thaha *et al.* [106] investigated the corrosion behavior of sintered MgZnFeCuCo alloys in Hanks' solution with and without 0.01 M coumarin. It was discovered that $Mg_{19}Zn_{17}Fe_{28}Cu_{18}Co$ exhibited main phases of Cu, Zn-rich phase regions of $MgZn_2$, $Mg_2Cu$, and $CuZn_5$. The microstructure of the $Mg_{11}Zn_{26}Fe_7Cu_4Co$ and $Mg_{11}Zn_6Fe_{0.2}Cu_{0.3}Co$ alloys contained $MgZn_2$, $Mg_2Cu$, $CuZn_5$, and FeZn, which were distributed along the grain boundaries of the respective alloys. The corrosion current density of $Mg_{19}Zn_{17}Fe_{28}Cu_{18}Co$ was the lowest when compared to $Mg_{11}Zn_{26}Fe_7Cu_4Co$ (313.5 μA·$cm^{-2}$) and $Mg_{11}Zn_6Fe_{0.2}Cu_{0.3}Co$ (345.6 μA·$cm^{-2}$). As a result, it demonstrated a superior corrosion resistance to $Mg_{11}Zn_{26}Fe_7Cu_4Co$ and $Mg_{11}Zn_6Fe_{0.2}Cu_{0.3}Co$ in Hanks' solution and Hanks' solution + 0.01 M coumarin. Furthermore, the corrosion resistance of MgZnFeCuCo alloys increased with an increase in the amounts of $MgZn_2$, $Mg_2Cu$, and $CuZn_5$ present in the α-Mg matrix of the alloy. The addition of 0.01 M coumarin inhibitor to the Hanks solution increased the charge resistance of all MgZnFeCuCo alloys regardless of their composition. This suggested that coumarin acted as a good corrosion inhibitor to protect the magnesium based HEAs $Mg_{19}Zn_{17}Fe_{28}Cu_{18}Co$, $Mg_{11}Zn_{26}Fe_7Cu_4Co$, and $Mg_{11}Zn_6Fe_{0.2}Cu_{0.3}Co$ from corrosion.

Singh *et al.* [107] conducted research to improve the corrosion resistance of mechanically alloyed FeCoCrNiCu HEA in 3.5% NaCl solution by the incorporation of carbon nanotubes (CNT). In the FeCoCrNiCu-CNT composites, two FCC phases (Cu-rich and Cr-rich) and a minor sigma phase were observed. The authors discovered that increasing the number of CNTs caused a progressive decrease in phase

separation. According to the corrosion resistance behavior of FeCoCrNiCu-CNT, it was observed that the corrosion rate increased with the addition of more CNTs to the composition. Basically, this implied that an optimal amount of CNT (2 wt%) could be used to incorporate into the HEA matrix to achieve a significant 88.6% reduction in the rate of corrosion. The improvement in corrosion resistance was attributed to an increase in chemical homogeneity, which reduced the likelihood of galvanic coupling occurring. Furthermore, the re-emergence of chemical heterogeneity and the evolution of the $Cr_{23}C_6$ phase were attributed to the increase in corrosion rate beyond the optimum CNT fraction.

A recent study conducted by Wang *et al.* [108] on the corrosion resistance of ball milled CuZrAlTiNiW/Al HEAs (designated as $Al_{10}$, $Al_{20}$, and $Al_{30}$) in artificial sea salt and distilled water (mass ratio = 1:30) led to an intriguing finding. A single BCC solid solution phase was found in the as-milled CuZrAlTiNiW, while the SPS-ed contained an ordered BCC phase (B2) along with $WAl_{12}$ intermetallic compound and a few unknown phases. Increases in the contents of $B_2$ and $WAl_{12}$ phases have been observed in HEAs as the volume fractions of the HEA alloys are increased from 10–30%. Potentiodynamic polarization curves revealed that $Al_{10}$ had the lowest corrosion current density ($i_{corr}$) of $0.86 \times 10^{-5}$ A·mm$^{-2}$ and the most positive corrosion potential ($E_{corr}$) of −1.04 V and lowest penetration rate of 0.827 mm per year, demonstrating that the use of high-efficiency additives could be beneficial in improving the general corrosion resistance of HEA composite materials. When compared to pure Al, the pitting resistance of the SPS-ed Al-HEA composites was significantly improved in seawater solution. The $Al_{30}$ composite, on the other hand, had the highest $\Delta E$ value (0.89 ± 0.05 V), indicating that it had a good pitting resistance.

## 4.4 Hydrogen storage

Hydrogen is being considered as a viable energy source in the development of cleaner energy to replace fossil fuels. Further improvements in this field are hinged on the development of safe and efficient hydrogen storage systems. It is possible to use metal hydrides in renewable energy systems because their compactness allows them to store large amounts of energy in relatively small spaces. They are also used in thermal energy storage systems and hydrogen compression [109]. In terms of properties, such as gravimetric/volumetric hydrogen storage capacity, heat of reaction, operating pressure, and temperature, selecting a suitable metal hydride is essential. The problem with metal hydrides composed of only transition metals is their limited capacity with a hydrogen/metal (H/M) gravimetric ratio ≤2 [110]. Because of the vast compositional space that can be evaluated in multicomponent systems, HEAs have attracted attention because of their ability to display a high hydrogen storage capacity with a H/M ratio of 2.5 [110,111]. They also have high lattice distortion, leading to additional lattice strain favorable for hydride formation. HEAs have shown a considerable amount of high hydrogen storage capacity of about 2.7 wt% using combinations of elements such as Ti, V, Zr, Nb, Ta, Hf, Nb, Al, and Ni as shown in Table 6.

Currently, the use of metal hydrides, such as magnesium (Mg) has attracted attention because of properties that favor hydrogen applications including high gravimetric capacity, lightweight, low cost, and abundance [112–114]. A few HEAs containing Mg synthesized by high-energy ball milling have already been reported and have displayed promising high hydrogen storage, as shown in Table 6. For example, $Mg_{0.68}TiNbNi_{0.55}$

**Table 6:** Hydrogen storage capacity of HEAs produced by arc-melting and high energy ball milling

| HEA | Production technique | Hydrogen absorption (wt%) | Hydrogen storage conditions (°C) | References |
|---|---|---|---|---|
| $Ti_{0.30}V_{0.25}Zr_{0.10}Nb_{0.25}Ta_{0.10}$ | Arc melting | 2.5 | 100 | [111] |
| TiVZrNbHf | Arc melting | 2.7 | 299 | [110] |
| TiZrNbCrFe | Arc melting | 1.9 | 200 | [165] |
| $Al_{0.10}Ti_{0.30}V_{0.25}Zr_{0.10}Nb_{0.25}$ | Arc melting | 2.6 | 25 | [111] |
| TiZrNbTa | Arc melting | 1.25 | 220 | [115] |
| $Ti_{0.20}Zr_{0.20}Hf_{0.20}Nb_{0.40}$ | Arc melting | 1.5 | 300 | [122] |
| MgTiVCrFe | High energy ball milling | 0.2 | 350 | [120] |
| MgVAlCrNi | High energy ball milling | 0.3 | 377 | [119] |
| $MgTiNbCr_{0.5}Mn_{0.5}Ni_{0.5}$ | High energy ball milling | 0.8 | 300 | [112] |
| $Mg_{0.68}TiNbNi_{0.55}$ | High energy ball milling | 3.3 | 380 | [112] |
| $MgZrTiFe_{0.5}Co_{0.5}Ni_{0.5}$ | High energy ball milling | 1.2 | 350 | [114] |

synthesized by high-energy ball milling had a high hydrogen storage of 3.3 wt% [112].

Strozi *et al.* [113] reported a method for designing a single-phase Mg-containing HEAs for hydrogen storage applications, which was performed *via* a high energy ball milling method for 24 h. A single-phase BCC crystal structure was discovered in the synthesized alloy ($Mg_{12}Al_{11}Ti_{33}Mn_{11}Nb_{33}$) using XRD, and further characterization with EDS revealed that the sample exhibited high chemical homogeneity. It was discovered that the lower temperature at which absorption occurs was 275°C for the initial pressure-composition-isotherm (PCI) test on $Mg_{12}Al_{11}Ti_{33}Mn_{11}Nb_{33}$ under hydrogen pressure of 30 bar. Based on their findings, it was estimated that the maximum hydrogen absorption capacity was approximately 1.75 wt% (H/M = 1.05). This value is higher than the hydrogen absorption capacity of reported $Ti_{0.20}Zr_{0.20}Hf_{0.20}Nb_{0.40}$ (1.5 wt% at 300°C) [114], $MgZrTiFe_{0.5}Co_{0.5}Ni_{0.5}$ (1.2 wt% at 350°C) [114], TiZrNbTa (1.25 wt% at 220°C) [115], and $MgTiNbCr_{0.5}Mn_{0.5}Ni_{0.5}$ (0.8 wt% at 300°C) [112]. The BCC phase found in $Mg_{12}Al_{11}Ti_{33}Mn_{11}Nb_{33}$ expanded following the PCI test. A mass loss of approximately 1.75 wt% was detected using TGA during the hydrogen desorption test, indicating that the hydrogen was completely dehydrated. After undergoing a hydrogen desorption test, a single BCC phase was revealed with two endothermic peaks that overlapped each other. There are two endothermic peaks that are associated with hydrogen release, the first of which is associated with the phase transformation of the undistorted BCC hydride (α-phase) and the second of which is associated with the hydrogen release from the α-Phase.

Cardoso *et al.* [116] produced another magnesium HEA (MgAlTiFeNi) by mechanical alloying (30 h at 200 rpm) and reactive milling (RM; 3 MPa for 24 h at 600 rpm). A primary BCC phase, an FCC phase ($TiH_2$), and a hydride phase ($Mg_2FeH_6$) were formed during the RM process. A BCC phase was formed during the mechanical alloying procedure. Using a DSC scan, it was discovered that the reactive milled-MgAlTiFeNi exhibited a hydrogen desorption peak at around 326°C. However, this was still lower and closer to the 378°C temperature determined for the pure complex hydride $Mg_2FeH_6$ [117]. The onset temperature for hydrogen desorption was 286°C, which was lower than the onset temperature for commercial magnesium hydride ($MgH_2$), which is between 426 and 442°C [118]. It was further discovered that the amount of hydrogen absorbed in the MgAlTiFeNi alloy by RM was 0.87 wt%, which increased to 0.94 wt% at 325°C after the second absorption, using the TG curve. These values were higher than reported hydrogen absorption capacities of high energy ball milled MgVAlCrNi at 0.3 wt% [119], $MgTiNbCr_{0.5}Mn_{0.5}Ni_{0.5}$ at 0.8 wt% [112], and MgTiVCrFe at 0.2 wt% [120]. However, the hydrogen absorption capacity was lower than as-cast $Ti_{0.30}V_{0.25}Zr_{0.10}Nb_{0.25}Ta_{0.10}$ at 2.5 wt% [121], $Al_{0.10}Ti_{0.30}V_{0.25}Zr_{0.10}Nb_{0.25}$ at 2.6 wt% [111], and $Ti_{0.20}Zr_{0.20}Hf_{0.20}Nb_{0.40}$ [122]. After desorption, it was discovered that the hydride-related peaks of $Mg_2FeH_6$ had disappeared, which indicated that the hydride had decomposed into Mg and Fe, as well as the release of hydrogen. All of the hydrogen that was removed from the reactive milled MgAlTiFeNi sample and detected by TG came from the decomposition of the $Mg_2FeH_6$.

## 4.5 Radiation application

Several promising properties of HEAs have been reported, including excellent combination of strength and ductility, as well as promising radiation-tolerant behavior [123,124]. Radiation resistance has been attributed to the complex intrinsic transport properties of HEAs where the increased compositional complexity can reduce effective interstitial mobility while increasing vacancy-interstitial reaction [125,126]. The mixing of various elements leads to the possibility of high irradiation resistance *via* unique “self-healing” mechanisms [127]. Similarly, Xia *et al.* [123] found that the "self-healing" process makes HEAs more stable against irradiation than other materials, like amorphous alloys and nano-structured alloys.

In the study of SPS-ed CuCrFeTiV irradiated at 300 keV at room temperature, Dias *et al.* [128] found that irradiation of CuCrFeTiV did not affect the microstructure. This behavior was reported by Kumar *et al.* [129] for an as-cast FeNiMnCrHEA, which retained its original crystalline structure after irradiation and dose up to 3 dpa at room temperature. In the as-cast HfNbTaTiZr alloy studied by Chang *et al.* [130], no phase transformation occurred after being irradiated with 300 keV $Ni^+$. These showed the high stability and resistance of CuCrFeTiV HEA to irradiation damage by energetic $Ar^+$ ions and to neutron irradiation in fusion reactors. Furthermore, Cui *et al.* [131] investigated the irradiation resistance of MA+SPS-ed $W_{90}(TaVCrTi)_{10}$, $W_{80}(TaVCrTi)_{20}$, $W_{70}(TaVCrTi)_{30}$, and $W_{60}(TaVCrTi)_{40}$ HEAs when exposed to 60 eV $He^+$ ion. The HEAs showed excellent surface stability when exposed to 60 eV $He^+$ ion irradiation. However, the $W_{70}(TaVCrTi)_{30}$ showed the best surface stability among the four HEAs. It was discovered that when the irradiation fluence was increased, the HEAs displayed a nearly flat surface irrespective of the irradiation fluence. The authors attributed the higher surface stability of the HEAs to their self-healing mechanism and ultrafine grain structure. The irradiation temperature did not significantly affect the HEAs, such that the irradiation damage of the $W_{60}(TaVCrTi)_{40}$ was slightly lower than that of the $W_{80}(TaVCrTi)_{20}$ and $W_{90}(TaVCrTi)_{10}$ alloys.

Zhou *et al.* [132] found that nanocrystalline $Al_xCoCrFeNi$ high-entropy alloys with varying Al concentrations ($x$ = 0, 1, 2) exhibited grain growth when subjected to a high-entropy radiation treatment. The HEAs were synthesized using a high-energy ball milling process that lasted 15 h, with ethanol serving as the wetting agent. High-entropy alloys made of nanocrystalline $Al_xCoCrFeNi$ were irradiated with 1 MeV $Kr^{2+}$ ions at room temperature. In the case of the nanocrystalline $Al_xCoCrFeNi$ HEAs, the crystal structure for $x$ = 0 was a simple FCC crystal structure, whereas the crystal structures for the other two Al concentrations ($x$ = 1 and $x$ = 2) were BCC + FCC crystal structures. The $Al_xCoCrFeNi$ HEAs studied by Zhou and co-workers experienced significant grain growth under 1 MeV $Kr^{2+}$ ions, with grain sizes increasing with irradiation dose from 13.8 ± 3, 7.4 ± 1, and 11± 1 nm before irradiation to 36 ± 8, 25 ± 5, and 26.6 ± 3 nm at an irradiation dose of 5.625 dpa. However, no phase transformation was found for the Al-0 alloy. While under ion irradiation, it was discovered that Al-2 alloy had the highest grain growth rate due to its lowest cohesive energy, which resulted in the lowest activation energy for atomic jump. According to the results of the irradiation test, a general trend of radiation-induced growth for nanocrystalline $Al_xCoCrFeNi$ high-entropy alloys was observed. The initial rapid grain growth of $Al_xCoCrFeNi$ high-entropy alloys was attributed to a disorder-driven mechanism caused by the loss of crystalline order because of ion-irradiation-induced large lateral damage volume. Relatively slow grain growth was attributed to the defect-driven mechanism near grain boundaries created by the radiation-induced point defects.

## 4.6 Thermoelectricity

Thermoelectric technology has attracted the interest of the scientific community due to its ability to convert heat into electricity in a solid state. It possesses a wide range of advantageous characteristics, including environmental friendliness, virtually no maintenance, zero noise, scalability, portability, and a long service life span [133]. High-entropy and medium-entropy alloys have intrinsically low lattice thermal conductivity due to effective scattering of phonons caused by lattice disorder, which results from the formation of lattice disorder in these alloys. The lead and tin chalcogenides PbTe, PbS, PbSe, SnTe, and SnS have all been proposed as promising and potentially thermoelectric materials, and their properties have been investigated.

According to Raphel *et al.* [134], the high entropy phenomena that resulted in low thermal conductivity in the $BiSbTe_{1.5}Se_{1.5}$ thermoelectric alloy are discussed. By combining mechanical alloying (5 h at 300 rpm) with SPS (325°C at 50 MPa), the $BiSbTe_{1.5}Se_{1.5}$ thermoelectric HEA was produced. In the case of mechanically alloyed HEA powder, the XRD peaks confirmed the presence of a monophase $BiSbTe_{1.5}Se_{1.5}$ alloy with a rhombohedral crystal structure. Since the alloy's absolute Seebeck coefficient ($S$) value was negative, it could be assumed to exhibit n-type semiconducting properties due to the contribution of electrons. In addition, the Seebeck coefficient increased with the increase in the temperature, rising from 117 $\mu V \cdot K^{-1}$ at 373 K to 124.97 $\mu V \cdot K^{-1}$ at 438 K. As the temperature was further increased, S decreased slightly, reaching 119.15 $\mu V \cdot K^{-1}$ at 523 K. Electrical conductivity ($\sigma$) increased monotonically from $2.85 \times 10^4$ $S \cdot m^{-1}$ at 373 K to $5.51 \times 10^4$ $S \cdot m^{-1}$ at 523 K, with the highest value occurring at 373 K. The enhanced configuration in $BiSbTe_{1.5}Se_{1.5}$ was due to the random and homogeneous atomic distribution, which could improve the crystal structure symmetry and electronic transport properties of the material [134]. In general, the high entropy and nanocrystalline features have a significant impact on the high configurational entropy because of the higher chemical disorder and lattice distortion in the material.

The thermoelectric properties of the block textured $BiSbTe_{1.5}Se_{1.5}$ HEA were investigated by Ivanov *et al.* [135]. The HEA was synthesized using SPS at 40 MPa and a temperature of 723 K for 15 min. The texturing axis was aligned with the direction of the SPS pressurization. The lamellar grain structure was formed because of the texturing process. The lamellar sheets did not cover the entire volume of the textured sample and are not continuous. Although there were blocks that contained continuous lamellar sheets that were oriented in a specific direction, the orientations of the sheets in neighboring blocks differed from one another. Specific electrical conductivity and thermal conductivity were measured perpendicularly and parallel to the texturing axis to determine the development of anisotropy because of the texturing process. Due to its low lattice thermal conductivity, the thermoelectric performance of the material was found to be suitably promising.

Kush *et al.* [136] studied the thermoelectric behavior of mechanical alloyed nickel base $Ni_2CuCrFeAl_x$ HEA and discovered that when the Al = 0.5, the Seebeck coefficient was 256.66 $\mu V \cdot K^{-1}$ at 660 K and then decreased to 35.06 $\mu V \cdot K^{-1}$ at 850 K. It was also found that when the Al content was greater than 0.5, there was an exponential rise in figure of merit ($ZT$) at ~0.2731 at 850 K. This indicated that the $ZT$ of $Ni_2CuCrFeAl_{0.5}$ alloy was strongly affected by Al-concentration. Tin telluride (SnTe) is a representative compound with a narrow bandgap and promising $ZT$ values. Yang *et al.* [137] enhanced the thermoelectric performance in

$Sn_{0.25}Pb_{0.25}Mn_{0.}25Ge_{0.25}Te$ HEAs through SnTe alloying and composition tuning. A *ZT* value of ~1.4 at 823 K was achieved, which was higher than the *ZT* value of 1.07 in $(Sn_{0.7}Ge_{0.2}Pb_{0.1})_{0.9}Mn_{0.11}Te$ HEAs [138]. At room temperature, the Seebeck coefficient increased to ~103 $\mu V \cdot K^{-1}$ higher than the 82 $\mu V \cdot K^{-1}$ recorded for $(Sn_{0.7}Ge_{0.2}Pb_{0.1})_{0.9}Mn_{0.11}Te$ HEAs [138].

In a separate study, Raphel *et al.* [139] investigated the synthesis of nanocrystalline PbSnTe HEA and $PbSn_{0\cdot875}TeSeBi_{0.125}$ HEA through mechanical alloying (5 h) and SPS (325°C). It was observed that the XRD peaks of sintered HEA samples corresponded to single-phase PbSnTeSe HEA with a NaCl type FCC crystal structure. The absolute Seebeck coefficient (*S*) result revealed that both the pristine and Bi-doped PbSnTeSe HEAs had S values in the positive range. This confirmed the p-type semiconducting behavior of the HEAs, with holes serving as the major charge carriers in both samples. The p-type semiconducting behavior was also observed by Fan *et al.* [140] in their study on the thermoelectric performance of PbSnTeSe high-entropy alloys. The peak value of S was also recorded at 623 K, with a value of 159.66 $\mu V \cdot K^{-1}$. In the nanocrystalline PbSnTeSe, substitutional doping of Bi caused the S to increase dramatically, reaching a maximum value of 194.85 $\mu V \cdot K^{-1}$ at 623 K. The increase in Seebeck coefficient that the thermoelectric alloy experienced was attributed to an increase in configurational entropy, which is believed to aid the modification of the alloy's band structure by increasing the phonon disorder. The electrical conductivity ($\sigma$) of the PbSnTeSe HEA gradually decreased from $6.13 \times 10^4$ $S \cdot m^{-1}$ at 373 K to $2.63 \times 10^4$ $S \cdot m^{-1}$ at 623 K, whereas the $PbSn_{0\cdot875}TeSeBi_{0.125}$ HEA gradually decreases from $5.95 \times 10^4$ $S \cdot m^{-1}$ at 373 K to the lowest value of $2.63 \times 10^4$ $S \cdot m^{-1}$ at 623 K. The high configurational entropy, higher chemical disorder, lattice distortion, and nanocrystalline features of both synthesized HEAs all contributed to achieving an ultralow thermal conductivity of less than 0.9 $W \cdot m^{-1} \cdot K^{-1}$ in both HEAs. It had a higher *ZT* of 0.71 than the PbSnTeSe HEA and very low thermal conductivity. This is because the band engineering makes it possible to get a high Seebeck coefficient and low thermal conductivity.

## 4.7 Deformation studies on PM processed-HEAs

To manufacture sheets, pipes, bars, and intricate parts from metallic alloys, hot forming technology, such as hot rolling or hot forging, is typically used. When metallic materials are subjected to hot deformation processes, their microstructures and properties can be enhanced, and the optimum parameters for processing such materials can be established. For example, good strength and ductility are often achieved during hot deformation processes due to grain refinement. It is for this reason that several researchers have used both experimental and computational techniques to provide further understanding of forming processing in many metallic systems. With respect to the processing of HEAs, most hot deformation studies were conducted on arc melted HEAs, with only a few studies on the hot deformation behavior of PM-HEAs. This may be ascribed to the near-net shaped processing nature of most PM components. The phenomena observed during hot forming behavior of PM-HEAs is like those of arc melted HEAs and conventional alloys. Some of the recent studies that focused on this topic are discussed in the subsequent paragraphs.

While assessing the hot deformation behavior of a MoNbTaTiV refractory HEA fabricated by PM, Liu *et al.* [141] identified that grain boundary gliding and rotation were the dominant deformation mechanisms when the alloy was deformed in the temperature range of 1,100–1,300°C and strain rate range of 0.0005–0.5 $s^{-1}$. After hot uniaxial compression testing, they found that the flow stresses were sensitive to the change in strain rate and deformation temperatures. When the deformation temperature was raised from 1,200 to 1,300°C, the maximum compressive stress was rapidly reduced at strain rates of 0.05 and 0.005 $s^{-1}$. Similar trends of compressive stress reduction at high temperatures were also reported in as-cast refractory HEAs (RHEAs) [142–144]. Furthermore, the microstructural characteristics of the deformed MoNbTaTiV alloy shown in Figure 9a reveal nearly-equiaxed grains, except for some deformation microstructures observed at 1,100–1,200°C and 0.05 $s^{-1}$ strain rate. Equiaxed grains microstructure have been reported for as-cast HEAs hot deformation at temperature of 1,000–1,100°C [145–147].

With the increase in deformation temperature and decrease in the strain rate, grain sizes increased though they were still ultrafine, suggesting the thermal stability of the RHEAs. This phenomenon was attributed to the characteristic sluggish diffusion effect caused by severe lattice distortion. As shown in the TEM images in Figure 9b, the grain boundaries of the deformed MoNbTaTiV RHEA are the nucleation sites for the ultrafine grains. Furthermore, smaller bulging shapes are observed to be present in Figure 9c. Consequently, several ultrafine discontinuous dynamic recrystallized grains are produced (Figure 9d). The bulging of grain boundaries, which was caused by the nucleation of new grains and subsequent grain growth, distinguished discontinuous dynamic crystallized grains from other types of crystallized grains [148]. The bulging phenomenon was also observed in some studies on the hot

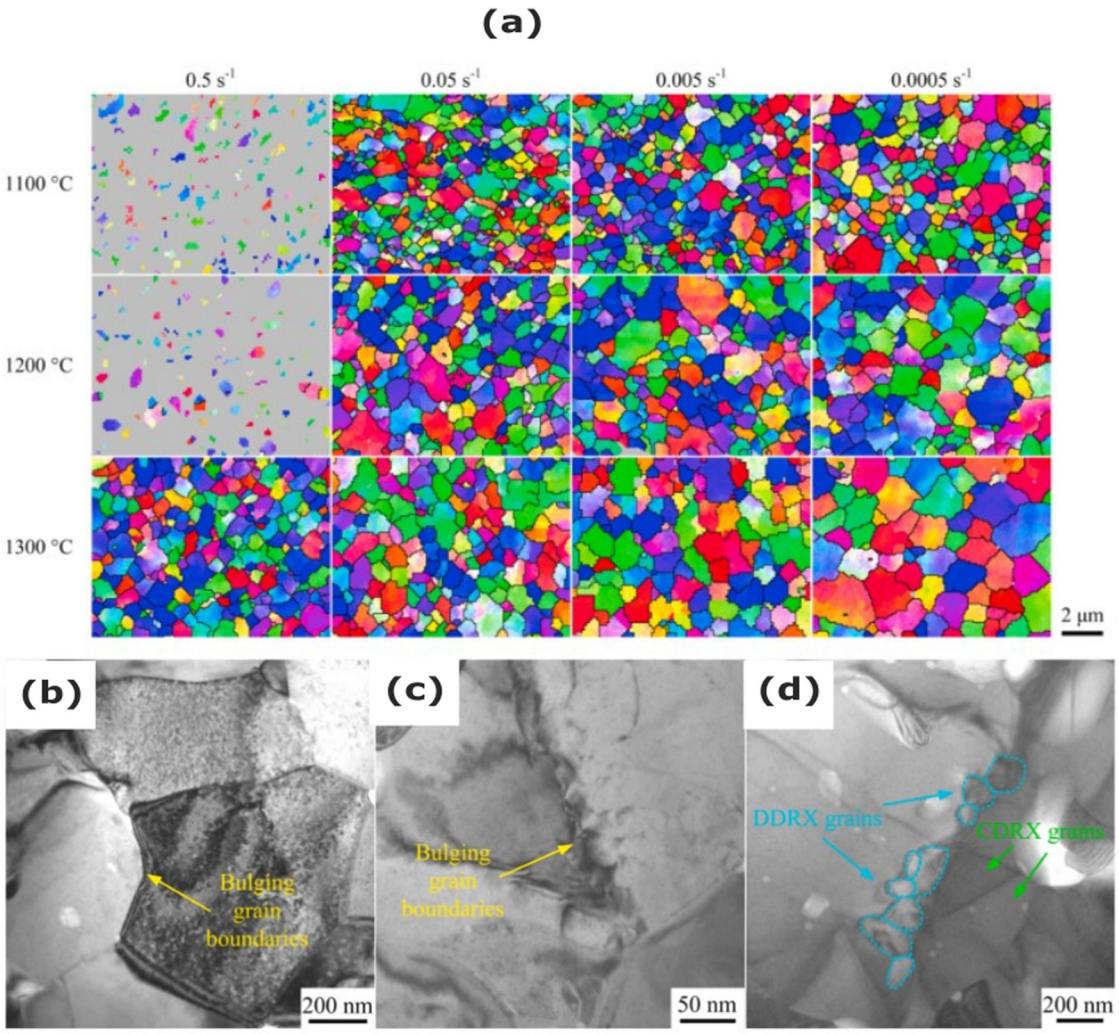


**Figure 9:** (a) Inverse pole figure maps of the deformed MoNbTaTiV RHEA at different deformation temperatures and strain rates and TEM images of the deformed MoNbTaTiV RHEA showing (b) and (c) bulging grain boundaries and (d) discontinuous dynamic crystallized grains and continuous dynamic crystallized grains. Reproduced with permission [141], Elsevier.

deformation of arc-melted RHEA alloys [143,144,149]. Severe extreme lattice distortion at the local grain boundaries, which has a strong pinning effect on the movement of the dislocations, can cause this phenomenon to occur. There is a restriction on the movement of grain boundaries during the bulging process, which leads to a very small bulging size [141].

Abhijit *et al.* [150] studied SRS in sintered CoCrFeMnNi HEA by nanoindentation. It was found that the SRS was negative (−0.0206), which was attributed to a cumulative effect of dislocation–grain boundary interaction, dislocation–interphase boundary interaction, dislocation–twin boundary interaction, and a highly frictional HEA lattice. Rymer *et al.* [151] investigated the SRS deformation behavior of sintered $Al_{0.3}$CrFeCoNi$Mo_{0.2}$ HEA under tension and compression at strain rates of $10^{-3}$, 10, and $10^{2}$ $s^{-1}$. It was discovered that the SRS of the deformed HEA was quite low, particularly when tensile loading was applied to it; 0.0072 at a plastic strain of 5% and 0.0066 at a plastic strain of 10%. For each investigated plastic strain, the SRS ($m$) value was 0.0149 at 5%, 0.0121 at 10%, and 0.0101 at 20% under compression. This was almost twice as high as deformation under tensile loading. A further observation was that, for both tension and compression, the SRS value showed a slight decrease with the increase in the plastic strain.

This is demonstrated by the fact that the $m$ value of the deformed HEA at a plastic strain of 20% under compression is approximately 33% lower than the $m$ value at 5% plastic strain. In as-cast $Al_{0.1}$CoCrFeNi HEA, the SRS of the flow stress changed from positive to zero to negative when tensile loading was applied. Therefore, the negative SRS was attributed to dynamic strain ageing of dislocations by the solutes created by aluminum atoms (Komarasamy

*et al.*, [152]). Likewise, in as-cast $Al_{0.3}$CoCrFeNi HEA, both negative SRS and dynamic strain ageing were observed [153]. This discovery demonstrated that the strain rate sensitive behavior was asymmetric in both tension and compression.

### 4.8 Summary of functional applications of PM-processed HEAs

The summary of important findings in some published articles (2019–2022) relating to corrosion, thermoelectric, oxidation, tribological, deformation, hydrogen storage, and radiation properties of PM-HEAs are presented below.

- It was revealed that the deformation temperature and the strain rate had a significant effect on the flow stresses. The dominant deformation mechanism was the discontinuous dynamic recrystallization mechanism. In addition, equiaxed grain microstructure and grain boundary bulging were found, which were comparable to as-cast HEAs during high temperature deformation. Negative SRS occurred in sintered HEAs like what was reported for as-cast HEAs.
- Existing PM-HEA literature showed that composition tuning and the addition of dopants, such as Bi and Ga, were instrumental in attaining a higher *ZT* value in HEA thermoelectric alloys. The dopants increased the bandgap and created a directional anisotropy effect, which increased the absolute Seebeck coefficient and ultralow thermal conductivity that resulted in a higher *ZT*.
- The addition of 10 wt% of $TiB_2$, $Cr_3C_2$, and $ZrO_2$ reinforcement particles in the CoCrFeNi HEA matrix increased its wear resistance. In addition, the hardness of HEAs was enhanced with the increase in the weight fractions of hard ceramic particles. The decrease in friction coefficient of the composite containing HEAs could be attributed to oxide layer formation and matrix softening effects at higher temperatures.
- As appears in as-cast HEAs, spallation due to high thermal stresses developed within the substrate and the oxide layer in PM-HEAs CoCrFeMnNi. The addition of Mn to FeCoCrNi resulted in the formation of Mn-based oxide scales, which did not provide protection against oxidation.
- It is worth noting that, due to its lightweight and its monohydride formability, the gravimetric capacity of the $Mg_{12}Al_{11}Ti_{33}Mn_{11}Nb_{33}$ alloy is still competitive with other refractory HEAs that form dihydrides. After hydrogen desorption in MgAlTiFeNi, it was found that the hydride-related peaks of $Mg_2FeH_6$ had disappeared, which meant that the hydride had decomposed into Mg and Fe with the simultaneous release of hydrogen gas.
- As the corrosion potential and current density increased, polarization resistance decreased with the increase in the annealing temperature. The formed sigma phase during the annealing process decreased the corrosion resistance of PM-HEAs. The addition of 0.01 M coumarin to Hanks' solution acted as a corrosion inhibitor and increased the charge resistance of all MgZnFeCuCo alloys regardless of their composition. A carbon nano tube of 2 wt% reduced the corrosion rate of FeCoCrNiCu HEA in a 3.5% NaCl solution.
- During the irradiation of SPS-ed CuCrFeTiV, higher surface stability was attributed to self-healing mechanism and ultrafine grain structure of HEA.

## 5 Suggested future works

This review shows that there is still a lot to learn about PM-HEAs and other processing methods like high-pressure torsion, magnetron sputtering, and additive manufacturing, which are rarely discussed but can be used to produce HEAs. Some of these future research areas are identified from the analysis of co-occurrence network of author keywords presented in "3.5 Co-occurrence network of author keywords" and review of functional applications discussed in Chapter 4. A summary of these future research focus in the PM processing of HEAs is presented below.

- There are no studies on the deformation mechanism of PM-HEA composites. This can be explored to determine if the deformation mechanism is analogous to as-cast HEA composites. No research was found discussing the constitutive equations and processing maps of PM-HEAs.
- For future study, more studies on compositional tuning and effects of dopants, such as Ag, Ga, La, and Bi on the thermal conductivity effect, Seebeck coefficient, and *ZT* attainment of multi-component thermoelectric alloys can be explored.
- Further research can be conducted on SPS-ed refractory HEAs containing hard ceramic particles to assess their tribological properties.
- Additionally, future research may be performed using small amounts of reactive elements such as La, Ce, Y, Hf, and Zr in preventing the oxidation resistance of PM-HEAs.
- More investigations are needed into the effects of the synthesis and processing methods on the hydrogen storage properties of Mg BCC HEAs. Some HEAs comprise

exceptionally high hydrogen absorption kinetic features. It will be interesting to study the influence of these HEAs on the hydrogen absorption kinetics of magnesium-based hydrogen storage alloys. Composition tuning may also be explored in designing promising hydrogen storage characteristics in high energy ball milled Mg-containing refractory HEAs. More studies are needed into the cyclic hydrogen absorption and desorption performance of ball milled Mg containing lightweight HEAs.

- Some studies have reported the use of additives (*e.g*., coumarin [106]) as corrosion inhibitors for MgZnFeCuCo HEAs. Due to the potential application of HEAs in the biomedical field, future studies may investigate other candidate corrosion inhibitors that are biocompatible.
- Singh *et al.* [107] reported a reduction in the corrosion rate of FeCoCrNiCu PM-HEAs through the incorporation of an optimal amount of CNT (2 wt%). Further studies can be conducted on the influence of 2 wt% CNTs on the corrosion rate of other PM-HEAs in chloride and acidic solutions.

# 6 Conclusion

This study bibliometrically analyzed the literature on PM processing of HEA/MCA between 2007 and 14th August 2022. Seven hundred research articles were extracted from the Scopus database and analyzed using the VOSviewer software. Results showed that more than a decade had elapsed since the first papers were published in the broad field of HEA/MCA before research attention focused on the PM processing of HEA/MCA. The foremost research outlets included *Journal of Alloys and Compounds, Materials Science and Engineering A, Materials Letters, Metals,* and *Intermetallics,* while the most prolific and highly cited authors were based in Chinese institutions. Nonetheless, inter-institutional research collaboration was very low, as indicated by co-authorship network analysis of research institutions. Furthermore, network mapping of co-occurrence of author keywords was used to identify existing and suggest future research directions and processing techniques, such as high-pressure torsion, magnetron sputtering, and additive manufacturing, which required further research inputs. Our analyses were derived from the bibliographic data of articles published in the English language; therefore, future bibliometric studies may consider articles published in other languages, merge research articles from different databases, and take other academic sources (*e.g*., conferences, books, and encyclopedia) into account. The results of this bibliometric study and systematic review of emerging functional areas will support experts in improving their knowledge of the field, readily identifying application areas needed extensive research, and enhance research collaboration across borders. Additionally, this study provides funding bodies and industry with the necessary information in allocating resources to research niches that will bring benefit to the society.

**Acknowledgments:** A.D.A appreciates the support from the Department of Metallurgical and Materials Engineering, Federal University of Technology, Akure.

**Funding information:** The authors state no funding involved.

**Author contributions**: A.D.A. and M.O.B. designed the methodology, while A.D.A. and O.S.B implemented it. A.D.A provided formal analysis and visualization, while A.D.A, O.S.B., and M.O.B. wrote the original draft. A.D.A. and M.O.B. completed the reviews. All authors have accepted responsibility for the entire content of this manuscript and approved its submission.

**Conflict of interest:** The authors state no conflict of interest.

**Data availability statement:** The datasets generated during and/or analyzed during the current study are available from the corresponding author on reasonable request.

# References

[1] Cantor, B., I. T. H. Chang, P. Knight, and A. J. B. Vincent. Microstructural development in equiatomic multicomponent alloys. *Materials Science and Engineering A*, Vol. 375–377, No. 1–2, SPEC. ISS. 2004, pp. 213–218.

[2] Yeh, J. W., S. K. Chen, S. J. Lin, J. Y. Gan, T. S. Chin, T. T. Shun, et al. Nanostructured high-entropy alloys with multiple principal elements: Novel alloy design concepts and outcomes. *Advanced Engineering Materials*, Vol. 6, No. 5, 2004, pp. 299–303.

[3] Takeuchi, A., T. Wada, and H. Kato. Solid Solutions with bcc , hcp , and fcc Structures Formed in a Composition Line in Multicomponent Ir–Rh–Ru–W–Mo System. *Materials Transactions*, Vol. 60, No. 11, 2019, pp. 2267–2276.

[4] Tang, J., J. L. Xu, Z. G. Ye, X. B. Li, and J. M. Luo. Microwave sintered porous CoCrFeNiMo high entropy alloy as an efficient electrocatalyst for alkaline oxygen evolution reaction. *Journal of Materials Science and Technology*, Vol. 79, 2021, pp. 171–177.

[5] Senkov, O. N., G. B. Wilks, D. B. Miracle, C. P. Chuang, and P. K. Liaw. Refractory high-entropy alloys. *Intermetallics*, Vol. 18, No. 9, 2010, pp. 1758–1765.

[6] Gao, M. C.. Progress in high-entropy alloys. *JOM*, Vol. 66, No. 10, 2014, pp. 1964–1965.

[7] Tsai, M. H. and J. W. Yeh. High-entropy alloys: A critical review. *Materials Research Letters*, Vol. 2, No. 3, 2014, pp. 107–123.

[8] Miracle, D. B. and O. N. Senkov. A critical review of high entropy alloys and related concepts. *Acta Materialia*, Vol. 122, 2017, pp. 448–511.
[9] Liu, L., J. B. Zhu, C. Hou, J. C. Li, and Q. Jiang. Dense and smooth amorphous films of multicomponent FeCoNiCuVZrAl high-entropy alloy deposited by direct current magnetron sputtering. *Materials and Design*, Vol. 46, 2013, pp. 675–679.
[10] Wu, H., S. Huang, H. Zhu, and Z. Xie. Strengthening FeCrNiCu high entropy alloys via combining V additions with in-situ TiC particles. *Scripta Materialia*, Vol. 195, 2021, id. 113724.
[11] Nagase, T., M. Todai, and T. Nakano. Development of Ti–Zr–Hf–Y–La high-entropy alloys with dual hexagonal-close-packed structure. *Scripta Materialia*, Vol. 186, 2020, pp. 242–246.
[12] Zhang, Y., T. T. Zuo, Z. Tang, M. C. Gao, K. A. Dahmen, P. K. Liaw, et al. Microstructures and properties of high-entropy alloys. *Progress in Materials Science*, Vol. 61, No. October 2013, 2014, pp. 1–93.
[13] Guo, S. and C. T. Liu. Phase stability in high entropy alloys: Formation of solid-solution phase or amorphous phase. *Progress in Natural Science: Materials International*, Vol. 21, No. 6, 2011, pp. 433–446.
[14] Shivam, V., J. Basu, V. K. Pandey, Y. Shadangi, and N. K. Mukhopadhyay. Alloying behaviour, thermal stability and phase evolution in quinary AlCoCrFeNi high entropy alloy. *Advanced Powder Technology*, Vol. 29, No. 9, 2018, pp. 2221–2230.
[15] Anand Sekhar, R., S. Samal, N. Nayan, and S. R. Bakshi. Microstructure and mechanical properties of Ti-Al-Ni-Co-Fe based high entropy alloys prepared by powder metallurgy route. *Journal of Alloys and Compounds*, Vol. 787, 2019, pp. 123–132.
[16] Vaidya, M., G. M. Muralikrishna, and B. S. Murty. High-entropy alloys by mechanical alloying: A review. *Journal of Materials Research*, Vol. 34, No. 5, 2019, pp. 664–686.
[17] Wu, Y., P. K. Liaw, and Y. Zhang. Preparation of bulk TiZrNbMoV and NbTiAlTaV high-entropy alloys by powder sintering. *Metals*, Vol. 11, No. 11, 2021, id. 1748.
[18] Oh, M. C., A. Sharma, H. Lee, and B. Ahn. Phase separation and mechanical behavior of AlCoCrFeNi-X (X = Cu, Mn, Ti) high entropy alloys processed via powder metallurgy. *Intermetallics*, Vol. 139, 2021, id. 107369.
[19] Liu, Q., G. Wang, X. Sui, Y. Xu, Y. Liu, and J. Yang. Ultra-fine grain TixVNbMoTa refractory high-entropy alloys with superior mechanical properties fabricated by powder metallurgy. *Journal of Alloys and Compounds*, Vol. 865, 2021, id. 158592.
[20] Chen, L., Z. Li, P. Dai, P. Fu, J. Chen, and Q. Tang. Effects of carbon addition on microstructure and mechanical properties of Fe50Mn30Co10Cr10 high-entropy alloy prepared by powder metallurgy. *Journal of Materials Research and Technology*, Vol. 20, 2022, pp. 73–87.
[21] Nagarjuna, C., K. Yong Jeong, Y. Lee, S. Min Woo, S. Ig Hong, H. Seop Kim, et al. Strengthening the mechanical properties and wear resistance of CoCrFeMnNi high entropy alloy fabricated by powder metallurgy. *Advanced Powder Technology*, Vol. 33, No. 4, 2022, id. 103519.
[22] Asghari-Rad, P., P. Sathiyamoorthi, N. T. C. Nguyen, A. Zargaran, T. S. Kim, and H. S. Kim. A powder-metallurgy-based fabrication route towards achieving high tensile strength with ultra-high ductility in high-entropy alloy. *Scripta Materialia*, Vol. 190, 2021, pp. 69–74.
[23] Chae, M. J., A. Sharma, M. C. Oh, and B. Ahn. Lightweight AlCuFeMnMgTi high entropy alloy with high strength-to-density ratio processed by powder metallurgy. *Metals and Materials International*, Vol. 27, No. 4, 2021, pp. 629–638.
[24] Ge, W., B. Wu, S. Wang, S. Xu, C. Shang, Z. Zhang, et al. Characterization and properties of CuZrAlTiNi high entropy alloy coating obtained by mechanical alloying and vacuum hot pressing sintering. *Advanced Powder Technology*, Vol. 28, No. 10, 2017, pp. 2556–2563.
[25] Liu, Y., J. Wang, Q. Fang, B. Liu, Y. Wu, and S. Chen. Preparation of superfine-grained high entropy alloy by spark plasma sintering gas atomized powder. *Intermetallics*, Vol. 68, 2016, pp. 16–22.
[26] Praveen, S., B. S. Murty, and R. S. Kottada. Phase evolution and densification behavior of nanocrystalline multicomponent high entropy alloys during spark plasma sintering. *JOM*, Vol. 65, No. 12, 2013, pp. 1797–1804.
[27] Varalakshmi, S., M. Kamaraj, and B. S. Murty. Synthesis and characterization of nanocrystalline AlFeTiCrZnCu high entropy solid solution by mechanical alloying. *Journal of Alloys and Compounds*, Vol. 460, No. 1–2, 2008, pp. 253–257.
[28] Ji, W., W. Wang, H. Wang, J. Zhang, Y. Wang, F. Zhang, et al. Alloying behavior and novel properties of CoCrFeNiMn high-entropy alloy fabricated by mechanical alloying and spark plasma sintering. *Intermetallics*, Vol. 56, 2015, pp. 24–27.
[29] Colombini, E., R. Rosa, L. Trombi, M. Zadra, A. Casagrande, and P. Veronesi. High entropy alloys obtained by field assisted powder metallurgy route: SPS and microwave heating. *Materials Chemistry and Physics*, Vol. 210, 2018, pp. 78–86.
[30] Mane, R. B., Y. Rajkumar, and B. B. Panigrahi. Sintering mechanism of CoCrFeMnNi high-entropy alloy powders. *Powder Metallurgy*, Vol. 61, No. 2, 2018, pp. 131–138.
[31] Joseph, J., N. Stanford, P. Hodgson, and D. M. Fabijanic. Tension/compression asymmetry in additive manufactured face centered cubic high entropy alloy. *Scripta Materialia*, Vol. 129, 2017, pp. 30–34.
[32] Fujieda, T., H. Shiratori, K. Kuwabara, T. Kato, K. Yamanaka, Y. Koizumi, et al. First demonstration of promising selective electron beam melting method for utilizing high-entropy alloys as engineering materials. *Materials Letters*, Vol. 159, 2015, pp. 12–15.
[33] Wu, W., R. Zhou, B. Wei, S. Ni, Y. Liu, and M. Song. Nanosized precipitates and dislocation networks reinforced C-containing CoCrFeNi high-entropy alloy fabricated by selective laser melting. *Materials Characterization*, Vol. 144, 2018, pp. 605–610.
[34] Brif, Y., M. Thomas, and I. Todd. The use of high-entropy alloys in additive manufacturing. *Scripta Materialia*, Vol. 99, 2015, pp. 93–96.
[35] Kumar, A., A. K. Swarnakar, and M. Chopkar. Phase evolution and mechanical properties of AlCoCrFeNiSix high-entropy alloys synthesized by mechanical alloying and spark plasma sintering. *Journal of Materials Engineering and Performance*, Vol. 27, No. 7, 2018, pp. 3304–3314.
[36] Veronesi, P., E. Colombini, R. Rosa, C. Leonelli, and F. Rosi. Microwave assisted synthesis of Si-modified Mn25FexNi25Cu(50−x) high entropy alloys. *Materials Letters*, Vol. 162, 2016, pp. 277–280.
[37] Varalakshmi, S., G. Appa Rao, M. Kamaraj, and B. S. Murty. Hot consolidation and mechanical properties of nanocrystalline equiatomic AlFeTiCrZnCu high entropy alloy after mechanical alloying. *Journal of Materials Science*, Vol. 45, No. 19, 2010, pp. 5158–5163.
[38] Torralba, J. M., P. Alvaredo, and A. García-Junceda. High-entropy alloys fabricated via. *powder metallurgy A critical review Powder Metallurgy*, Vol. 62, No. 2, 2019, pp. 84–114.

[39] Torralba, J. M. and M. Campos. High entropy alloys manufactured by additive manufacturing. *Metals*, Vol. 10, No. 5, 2020.
[40] van Eck, N. J. and L. Waltman. Visualizing Bibliometric Networks. In *Measuring Scholarly Impact*, Y. Ding, Rousseau, R., Wolfram, D., (Eds.), Springer, Cham, pp. 285–320.
[41] Pritchard, A. Statistical bibliography or bibliometrics? *Journal of Documentation 4*, Vol. Vol. 25, Accessed Dec. 16, 2022, pp. 348–349.
[42] Mingers, J. and L. Leydesdorff. A review of theory and practice in scientometrics. *European Journal of Operational Research*, Vol. 246, No. 1, 2015, pp. 1–19.
[43] Garfield, E. Citation indexes for science. A new dimension in documentation through association of ideas. *Science*, Vol. 122, No. 3159, 1955, pp. 108–111.
[44] Garfield, E. From the science of science to Scientometrics visualizing the history of science with HistCite software. *Journal of Informetrics*, Vol. 3, No. 3, 2009, pp. 173–179.
[45] Bornmann, L. and L. Leydesdorff. Scientometrics in a changing research landscape. *EMBO reports*, Vol. 15, No. 12, 2014, pp. 1223–1330.
[46] Hussein, M. and T. Zayed. Crane operations and planning in modular integrated construction: Mixed review of literature. *Automation in Construction*, Vol. 122, 2021, id. 103466.
[47] Chang, Y. W., M. H. Huang, and C. W. Lin. Evolution of research subjects in library and information science based on keyword, bibliographical coupling, and co-citation analyses. *Scientometrics*, Vol. 105, No. 3, 2015, pp. 2071–2087.
[48] Heersmink, R., J. van den Hoven, N. J. van Eck, and J. Den van Berg. Bibliometric mapping of computer and information ethics. *Ethics and Information Technology*, Vol. 13, No. 3, 2011, pp. 241–249.
[49] van Eck, N. J. and L. Waltman. Bibliometric mapping of the computational intelligence field. *International Journal of Uncertainty, Fuzziness and Knowlege-Based Systems*, Vol. 15, No. 5, 2007, pp. 625–645.
[50] Kokol, P., H. Blažun Vošner, and J. Završnik. Application of bibliometrics in medicine: a historical bibliometrics analysis. *Health Information and Libraries Journal*, Vol. 38, No. 2, 2021, pp. 125–138.
[51] Md Khudzari, J., J. Kurian, B. Tartakovsky, and G. S. V. Raghavan. Bibliometric analysis of global research trends on microbial fuel cells using Scopus database. *Biochemical Engineering Journal*, Vol. 136, 2018, pp. 51–60.
[52] Xing, Y., Z. Ma, W. Su, Q. Wang, X. Wang, and H. Zhang. Analysis of research status of CO2 conversion technology based on bibliometrics. *Catalysts*, Vol. 10, No. 370, 2020, pp. 1–18.
[53] van Eck, N. J. and L. Waltman. Software survey: VOSviewer, a computer program for bibliometric mapping. *Scientometrics*, Vol. 84, No. 2, 2010, pp. 523–538.
[54] *Google Inc. OpenRefine: A free, open source, powerful tool for working with messy data*, 2021.
[55] Liskiewicz, T., G. Liskiewicz, and J. Paczesny. Factors affecting the citations of papers in tribology journals. *Scientometrics*, Vol. 126, No. 4, 2021, pp. 3321–3336.
[56] Tahamtan, I., A. S. Askar, and K. Ahamdzadeh. Factors affecting number of citations: a comprehensive review of the literature. *Scientometrics*, Vol. 107, 2016, pp. 1195–1225.
[57] van Eck, N. J. and L. Waltman. VOSviewer Manual version 1.6.16. *Univeristeit Leiden November*, pp. 1–52.
[58] Akinwekomi, A. D. and F. Akhtar. Bibliometric mapping of literature on high-entropy/multicomponent alloys and systematic review of emerging applications. *Entropy*, Vol. 24, No. 3, 2022, id. 329.
[59] Hsu, U. S., U. D. Hung, J. W. Yeh, S. K. Chen, Y. S. Huang, and C. C. Yang. Alloying behavior of iron, gold and silver in AlCoCrCuNi-based equimolar high-entropy alloys. *Materials Science and Engineering A*, Vol. 460–461, 2007, pp. 403–408.
[60] Chen, Y. L., Y. H. Hu, C. A. Hsieh, J. W. Yeh, and S. K. Chen. Competition between elements during mechanical alloying in an octonary multi-principal-element alloy system. *Journal of Alloys and Compounds*, Vol. 481, No. 1–2, 2009, pp. 768–775.
[61] Liu, W. H., Z. P. Lu, J. Y. He, J. H. Luan, Z. J. Wang, B. Liu, et al. Ductile CoCrFeNiMox high entropy alloys strengthened by hard intermetallic phases. *Acta Materialia*, Vol. 116, 2016, pp. 332–342.
[62] Senkov, O. N., S. V. Senkova, and C. Woodward. Effect of aluminum on the microstructure and properties of two refractory high-entropy alloys. *Acta Materialia*, Vol. 68, 2014, pp. 214–228.
[63] Youssef, K. M., A. J. Zaddach, C. Niu, D. L. Irving, and C. C. Koch. A novel low-density, high-hardness, high-entropy alloy with close-packed single-phase nanocrystalline structures. *Materials Research Letters*, Vol. 3, No. 2, 2014, pp. 95–99.
[64] Praveen, S., B. S. Murty, and R. S. Kottada. Alloying behavior in multi-component AlCoCrCuFe and NiCoCrCuFe high entropy alloys. *Materials Science and Engineering: A*, Vol. 534, 2012, pp. 83–89.
[65] Senkov, O. N. and C. F. Woodward. Microstructure and properties of a refractory NbCrMo0.5Ta0.5TiZr alloy. *Materials Science and Engineering A*, Vol. 529, No. 1, 2011, pp. 311–320.
[66] Akinwekomi, A. D., W.-C. Law, C.-Y. Tang, L. Chen, and C.-P. Tsui. Rapid microwave sintering of carbon nanotube-filled AZ61 magnesium alloy composites. *Composites Part B: Engineering*, Vol. 93, 2016, pp. 302–309.
[67] Akinwekomi, A. D., C. Tang, G. C. Tsui, W. Law, L. Chen, X. Yang, et al. Synthesis and characterisation of floatable magnesium alloy syntactic foams with hybridised cell morphology. *Materials & Design*, Vol. 160, 2018, pp. 591–600.
[68] Jayalakshmi, S., S. Gupta, S. Sankaranarayanan, S. Sahu, and M. Gupta. Structural and mechanical properties of Ni60Nb40 amorphous alloy particle reinforced Al-based composites produced by microwave-assisted rapid sintering. *Materials Science and Engineering A*, Vol. 581, 2013, pp. 119–127.
[69] Dai, D., T. Xu, X. Wei, G. Ding, Y. Xu, J. Zhang, et al. Using machine learning and feature engineering to characterize limited material datasets of high-entropy alloys. *Computational Materials Science*, Vol. 175, No. February, 2020, id. 109618.
[70] Xiong, J., S. Q. Shi, and T. Y. Zhang. Machine learning of phases and mechanical properties in complex concentrated alloys. *Journal of Materials Science and Technology*, Vol. 87, 2021, pp. 133–142.
[71] Akinwekomi, A. D. and A. I. Lawal. Neural network-based model for predicting particle size of AZ61 powder during high-energy mechanical milling. *Neural Computing and Applications*, Vol. 33, 2021, pp. 17611–17619.
[72] Conduit, B. D., N. G. Jones, H. J. Stone, and G. J. Conduit. Design of a nickel-base superalloy using a neural network. *Materials & Design*, Vol. 131, 2017, pp. 358–365.
[73] Durga, A., K. C. Hari Kumar, and B. S. Murty. Phase formation in equiatomic high entropy alloys: CALPHAD approach and experimental studies. *Transactions of the Indian Institute of Metals*, Vol. 65, No. 4, 2012, pp. 375–380.
[74] Sun, W., X. Huang, and A. A. Luo. Phase formations in low density high entropy alloys. *Calphad*, Vol. 56, 2017, pp. 19–28.

[75] Huang, W., P. Martin, and H. L. Zhuang. Machine-learning phase prediction of high-entropy alloys. *Acta Materialia*, Vol. 169, 2019, pp. 225–236.
[76] Wen, C., Y. Zhang, C. Wang, D. Xue, Y. Bai, S. Antonov, et al. Machine learning assisted design of high entropy alloys with desired property. *Acta Materialia*, Vol. 170, 2019, pp. 109–117.
[77] Torralba, J. M., P. Alvaredo, and A. García-Junceda. Powder metallurgy and high-entropy alloys: update on new opportunities. *Powder Metallurgy*, Vol. 63, No. 4, 2020, pp. 227–236.
[78] Zhou, J. L., Y. H. Cheng, Y. X. Chen, and X. B. Liang. Composition design and preparation process of refractory high-entropy alloys: A review. *International Journal of Refractory Metals and Hard Materials*, Vol. 105, No. December 2021, 2022, id. 105836.
[79] Karan, P., A. Pachauri, Kumar, and M. Maurya. Effect of powder metallurgy on high entropy alloy materials: A review. *Materials Today: Proceedings*, Vol. 47, 2021, pp. 4026–4033.
[80] Moravcikova-Gouvea, L., I. Moravcik, M. Omasta, J. Veselý, J. Cizek, P. Minárik, et al. High-strength Al0.2Co1.5CrFeNi1.5Ti high-entropy alloy produced by powder metallurgy and casting: A comparison of microstructures, mechanical and tribological properties. *Materials Characterization*, Vol. 159, No. November 2019, 2020, id. 110046.
[81] Kang, J. G., B. T. Yang, and J. C. Wei. Effect of TiB2 on the Phase Composition, Microstructure, and Tribological Properties of AlCoCrFeNi/TiB2 Composites. *Powder Metallurgy and Metal Ceramics*, Vol. 59, No. 9–10, 2021, pp. 537–545.
[82] Zou, H., X. Ran, W. Zhu, Y. Wang, S. Zhan, and Z. Hao. Tribological behavior of copper-graphite composites reinforced with Cu-coated or uncoated SiO2 particles. *Materials*, Vol. 11, No. 12, 2018, pp. 1–12.
[83] Ravindran, P., K. Manisekar, R. Narayanasamy, and P. Narayanasamy. Tribological behaviour of powder metallurgy-processed aluminium hybrid composites with the addition of graphite solid lubricant. *Ceramics International*, Vol. 39, No. 2, 2013, pp. 1169–1182.
[84] Guo, Z., A. Zhang, J. Han, and J. Meng. Microstructure, mechanical and tribological properties of CoCrFeNiMn high entropy alloy matrix composites with addition of Cr3C2. *Tribology International*, Vol. 151, 2020, pp. 1–11.
[85] Ghanbariha, M., M. Farvizi, T. Ebadzadeh, and A. Alizadeh Samiyan. Effect of ZrO2 particles on the nanomechanical properties and wear behavior of AlCoCrFeNi–ZrO2 high entropy alloy composites. *Wear*, Vol. 484–485, 2021, pp. 1–15.
[86] Wang, L., Y. Geng, A. K. Tieu, G. Hai, H. Tan, J. Chen, et al. In-situ formed graphene providing lubricity for the FeCoCrNiAl based composite containing graphite nanoplate. *Composites Part B: Engineering*, Vol. 221, 2021, pp. 1–14.
[87] Prabhu, T. R., M. Arivarasu, Y. Chodancar, N. Arivazhagan, G. Sumanth, and R. K. Mishra. Tribological behaviour of graphite-reinforced FeNiCrCuMo high-entropy alloy self-lubricating composites for aircraft braking energy applications. *Tribology Letters*, Vol. 67, No. 3, 2019, pp. 1–15.
[88] Anne, B. R., S. Shaik, M. Tanaka, and A. Basu. A crucial review on recent updates of oxidation behavior in high entropy alloys. *SN Applied Sciences*, Vol. 3, No. 3, 2021, pp. 1–23.
[89] Butler, T. M. and M. L. Weaver. Oxidation behavior of arc melted AlCoCrFeNi multi-component high-entropy alloys. *Journal of Alloys and Compounds*, Vol. 674, 2016, pp. 229–244.
[90] Chen, H., A. Kauffmann, B. Gorr, D. Schliephake, C. Seemüller, J. N. Wagner, et al. Microstructure and mechanical properties at elevated temperatures of a new Al-containing refractory high-entropy alloy Nb-Mo-Cr-Ti-Al. *Journal of Alloys and Compounds*, Vol. 661, 2016, pp. 206–215.
[91] Vilémová, M., H. Hadraba, Z. Weiss, F. Lukáč, Š. Csáki, Z. Chlup, et al. Phase, composition and structure changes of CoCrNi-based concentrated alloys resulting from high temperature oxidation. *Materials*, Vol. 13, No. 10, 2020, pp. 1–13.
[92] Holcomb, G. R., J. Tylczak, and C. Carney. Oxidation of CoCrFeMnNi High Entropy Alloys. *JOM 2015 67:10*, Vol. 67, No. 10, 2015, pp. 2326–2339.
[93] Esmaily, M., Y. Qiu, S. Bigdeli, M. B. Venkataraman, A. Allanore, and N. Birbilis. High-temperature oxidation behaviour of AlxFeCrCoNi and AlTiVCr compositionally complex alloys. *npj Materials Degradation*, Vol. 4, No. 1, 2020, pp. 1–10.
[94] Ostovari Moghaddam, A., N. A. Shaburova, M. N. Samodurova, A. Abdollahzadeh, and E. A. Trofimov. Additive manufacturing of high entropy alloys: A practical review. *Journal of Materials Science & Technology*, Vol. 77, 2021, pp. 131–162.
[95] Garip, Y., N. Ergin, and O. Ozdemir. Resistance sintering of CoCrFeNiAlx (x = 0.7, 0.85, 1) high entropy alloys: Microstructural characterization, oxidation and corrosion properties. *Journal of Alloys and Compounds*, Vol. 877, 2021, pp. 1–19.
[96] Kai, W., F. P. Cheng, Y. R. Lin, C. W. Chuang, R. T. Huang, D. Chen, et al. The oxidation behavior of Ni2FeCoCrAlx high-entropy alloys in dry air. *Journal of Alloys and Compounds*, Vol. 836, 2020, pp. 1–12.
[97] Gawel, R., J. Rogal, M. Dąbek, Wójcik-Bania, and K. Przybylski. High temperature oxidation behaviour of non-equimolar AlCoCrFeNi high entropy alloys. *Vacuum*, Vol. 184, 2021, id. 109969.
[98] Zhang, R., J. Meng, J. Han, K. Tulugan, and R. Zhang. Oxidation resistance properties of refractory high-entropy alloys with varied AlxCrTiMo content. *Journal of Materials Science*, Vol. 56, No. 4, 2021, pp. 3551–3561.
[99] Wang, K., A. D. Lan, and J. W. Qiao. Corrosion behavior of Al0.1CoCrFeNi high entropy alloy in various chloride-containing solutions. *Frontiers in Materials*, Vol. 7, 2021, id. 488.
[100] Abdelghafar, K. A., M. M. Ibrahim, M. A. Shoeib, and M. A. Waly. Evaluation of microstructural and corrosion resistance of as-cast Cu45Mn25Al15Fe5Cr5Ni5 high entropy alloy. *Materials Research Express*, Vol. 7, No. 1, 2020, id. 016579.
[101] Ren, B., Z. X. Liu, D. M. Li, L. Shi, B. Cai, and M. X. Wang. Corrosion behavior of CuCrFeNiMn high entropy alloy system in 1M sulfuric acid solution. *Materials and Corrosion*, Vol. 63, No. 9, 2012, pp. 828–834.
[102] Zhou, P. F., D. H. Xiao, and T. C. Yuan. Microstructure, mechanical and corrosion properties of AlCoCrFeNi high-entropy alloy prepared by spark plasma sintering. *Acta Metallurgica Sinica (English Letters)*, Vol. 33, No. 7, 2020, pp. 937–946.
[103] Shang, X. L., Z. J. Wang, Q. F. Wu, J. C. Wang, J. J. Li, and J. K. Yu. Effect of Mo addition on corrosion behavior of high-entropy alloys CoCrFeNiMo x in aqueous environments. *Acta Metallurgica Sinica (English Letters)*, Vol. 32, No. 1, 2019, pp. 41–51.
[104] Han, Z., W. Ren, J. Yang, A. Tian, Y. Du, G. Liu, et al. The corrosion behavior of ultra-fine grained CoNiFeCrMn high-entropy alloys. *Journal of Alloys and Compounds*, Vol. 816, 2020, id. 152583.
[105] Parakh, A., M. Vaidya, N. Kumar, R. Chetty, and B. S. Murty. Effect of crystal structure and grain size on corrosion properties of AlCoCrFeNi high entropy alloy. *Journal of Alloys and Compounds*, Vol. 863, 2021, id. 158056.

[106] Thaha, Y. N., I. Kartika, F. P. Lestari, A. N. Syahid, T. Asmaria, A. M. Ashari, et al. Corrosion behavior of MgZnFeCuCo alloys in the presence of coumarin. *Materials Today Communications*, Vol. 29, 2021, pp. 1–9.

[107] Singh, S., S. M. Shaikh, P. K. MK, B. S. Murty, and C. Srivastava. Microstructural homogenization and substantial improvement in corrosion resistance of mechanically alloyed FeCoCrNiCu high entropy alloys by incorporation of carbon nanotubes. *Materialia*, Vol. 14, 2020, pp. 1–11.

[108] Wang, N., B. Wu, W. Wu, J. Li, C. Ge, Y. Dong, et al. Microstructure and properties of aluminium-high entropy alloy composites fabricated by mechanical alloying and spark plasma sintering. *Materials Today Communications*, Vol. 25, 2020, pp. 1–8.

[109] Manickam, K., P. Mistry, G. Walker, D. Grant, C. E. Buckley, T. D. Humphries, et al. Future perspectives of thermal energy storage with metal hydrides. *International Journal of Hydrogen Energy*, Vol. 4415, 2019, pp. 7738–7745.

[110] Sahlberg, M., D. Karlsson, C. Zlotea, and U. Jansson. Superior hydrogen storage in high entropy alloys. *Scientific Reports*, Vol. 6, 2016, pp. 1–6.

[111] Montero, J., G. Ek, L. Laversenne, V. Nassif, C. Zlotea, J. Montero, et al. How 10 at % Al Addition in the Ti-V-Zr-Nb High-Entropy Alloy Changes Hydrogen Sorption Properties. *Molecules*, Vol. 26, No. 2470, 2021, pp. 1–12.

[112] Marques, F., H. C. Pinto, S. J. A. Figueroa, F. Winkelmann, M. Felderhoff, W. J. Botta, et al. Mg-containing multi-principal element alloys for hydrogen storage: A study of the MgTiNbCr0.5Mn0.5Ni0.5 and Mg0.68TiNbNi0.55 compositions. *International Journal of Hydrogen Energy*, Vol. 45, No. 38, 2020, pp. 19539–19552.

[113] Strozi, R. B., D. R. Leiva, J. Huot, W. J. Botta, and G. Zepon. An approach to design single BCC Mg-containing high entropy alloys for hydrogen storage applications. *International Journal of Hydrogen Energy*, Vol. 46, No. 50, 2021, pp. 25555–25561.

[114] Zepon, G., D. R. Leiva, R. B. Strozi, A. Bedoch, S. J. A. Figueroa, T. T. Ishikawa, et al. Hydrogen-induced phase transition of MgZrTiFe0.5Co0.5Ni0.5 high entropy alloy. *International Journal of Hydrogen Energy*, Vol. 43, No. 3, 2018, pp. 1702–1708.

[115] Zhang, C., A. Song, Y. Yuan, Y. Wu, P. Zhang, Z. Lu, et al. Study on the hydrogen storage properties of a TiZrNbTa high entropy alloy. *International Journal of Hydrogen Energy*, Vol. 45, No. 8, 2020, pp. 5367–5374.

[116] Cardoso, K. R., V. Roche, A. M. Jorge, F. J. Antiqueira, G. Zepon, and Y. Champion. Hydrogen storage in MgAlTiFeNi high entropy alloy. *Journal of Alloys and Compounds*, Vol. 858, 2021, id. 158357.

[117] Zhang, X., R. Yang, J. Qu, W. Zhao, L. Xie, W. Tian, et al. The synthesis and hydrogen storage properties of pure nanostructured Mg2FeH6. *Nanotechnology*, Vol. 21, No. 9, 2010, pp. 1–8.

[118] Silva, R. A., R. M. Leal Neto, D. R. Leiva, T. T. Ishikawa, C. S. Kiminami, A. M. Jorge, et al. Room temperature hydrogen absorption by Mg and Mg–TiFe nanocomposites processed by high-energy ball milling. *International Journal of Hydrogen Energy*, Vol. 43, No. 27, 2018, pp. 12251–12259.

[119] Strozi, R. B., D. R. Leiva, J. Huot, W. J. Botta, and G. Zepon. Synthesis and hydrogen storage behavior of Mg–V–Al–Cr–Ni high entropy alloys. *International Journal of Hydrogen Energy*, Vol. 46, No. 2, 2021, pp. 2351–2361.

[120] de Marco, M. O., Y. Li, H. W. Li, K. Edalati, and R. Floriano. Mechanical Synthesis and Hydrogen Storage Characterization of MgVCr and MgVTiCrFe High-Entropy Alloy. *Advanced Engineering Materials*, Vol. 22, No. 2, 2020.

[121] Montero, J., G. Ek, M. Sahlberg, and C. Zlotea. Improving the hydrogen cycling properties by Mg addition in Ti-V-Zr-Nb refractory high entropy alloy. *Scripta Materialia*, Vol. 194, 2021, id. 113699.

[122] Zhang, J., P. Li, G. Huang, W. Zhang, J. Hu, H. Xiao, et al. Superior hydrogen sorption kinetics of ti0.20 zr0.20 hf0.20 nb0.40 high-entropy alloy. *Metals*, Vol. 11, No. 3, 2021, pp. 1–16.

[123] Xia, S. Q., Z. Wang, T. F. Yang, Y. Zhang. Irradiation behavior in high entropy alloys. *Journal of Iron and Steel Research International*, Vol. 22, 2015, pp. 879–884.

[124] Lu, C., L. Niu, N. Chen, K. Jin, T. Yang, P. Xiu, et al. Enhancing radiation tolerance by controlling defect mobility and migration pathways in multicomponent single-phase alloys. *Nature Communications*, Vol. 7, 2016, pp. 1–8.

[125] Yang, T. C., G. Lu, K. Velisa, P. Jin, Y. Xiu, H. B. Zhang, et al. Influence of irradiation temperature on void swelling in NiCoFeCrMn and NiCoFeCrPd. *Scripta Materialia*, Vol. 158, 2019, pp. 57–61.

[126] Osetsky, Y. N., L. K. Béland, A. V. Barashev, and Y. Zhang. On the existence and origin of sluggish diffusion in chemically disordered concentrated alloys. *Current Opinion in Solid State and Materials Science*, Vol. 22, No. 3, 2018, pp. 65–74.

[127] Egami, T., M. Ojha, O. Khorgolkhuu, D. M. Nicholson, and G. M. Stocks. Local electronic effects and irradiation resistance in high-entropy alloys. *JOM*, Vol. 67, No. 10, 2015, pp. 2345–2349.

[128] Dias, M., F. Antão, N. Catarino, A. Galatanu, M. Galatanu, P. Ferreira, et al. Sintering and irradiation of copper-based high entropy alloys for nuclear fusion. *Fusion Engineering and Design*, Vol. 146, 2019, pp. 1824–1828.

[129] Kumar, N. A. P. K., C. Li, K. J. Leonard, H. Bei, and S. J. Zinkle. Microstructural stability and mechanical behavior of FeNiMnCr high entropy alloy under ion irradiation. *Acta Materialia*, Vol. 113, 2016, pp. 230–244.

[130] Chang, S., K.-K. Tseng, T.-Y. Yang, D.-S. Chao, J.-W. Yeh, and J.-H. Liang. Irradiation-induced swelling and hardening in HfNbTaTiZr refractory high-entropy alloy. *Materials Letters*, Vol. 272, 2020, id. 127832.

[131] Cui, H., N. Liu, L. Luo, Y. Xu, J. Cheng, and Y. Wu. Behavior of high-entropy W-rich alloys Wx(TaVCrTi)y under He+ irradiation. *Fusion Engineering and Design*, Vol. 172, 2021, id. 112904.

[132] Zhou, J., M. I. Islam, S. Guo, Y. Zhang, and F. Lu. Radiation-induced grain growth of nanocrystalline alxcocrfeni high-entropy alloys. *Journal of Physical Chemistry C*, Vol. 125, No. 6, 2021, pp. 3509–3516.

[133] Zhang, X. and L. D. Zhao. Thermoelectric materials: Energy conversion between heat and electricity. *Journal of Materiomics*, Vol. 1, No. 2, 2015, pp. 92–105.

[134] Raphel, A., P. Vivekanandhan, and S. Kumaran. High entropy phenomena induced low thermal conductivity in BiSbTe1.5Se1.5 thermoelectric alloy through mechanical alloying and spark plasma sintering. *Materials Letters*, Vol. 269, 2020, pp. 1–4.

[135] Ivanov, O., M. Yaprintsev, A. Vasil'ev, and E. Yaprintseva. Microstructure and thermoelectric properties of the medium-entropy block-textured BiSbTe1.5Se1.5 alloy. *Journal of Alloys and Compounds*, Vol. 872, 2021, pp. 1–7.

[136] Kush, L., S. Srivastava, Y. Jaiswal, and Y. Srivastava. Thermoelectric behaviour with high lattice thermal conductivity of Nickel base Ni2CuCrFeAlx (x = 0.5, 1.0, 1.5 and 2.5) high entropy alloys. *Materials Research Express*, Vol. 7, No. 3, 2020, id. 035704.

[137] Yang, J., J. Cai, R. Wang, Z. Guo, X. Tan, G. Liu, et al. Entropy engineering realized ultralow thermal conductivity and high seebeck coefficient in lead-free SnTe. *ACS Applied Energy Materials*, Vol. 4, No. 11, 2021, pp. 12738–12744.

[138] Hu, L., Y. Zhang, H. Wu, J. Li, Y. Li, M. Mckenna, et al. Entropy engineering of SnTe: Multi-principal-element alloying leading to ultralow lattice thermal conductivity and state-of-the-art thermoelectric performance. *Advanced Energy Materials*, Vol. 8, No. 29, 2018, id. 1802116.

[139] Raphel, A., A. K. Singh, P. Vivekanandhan, and S. Kumaran. Thermoelectric performance of nanostructured PbSnTeSe high entropy thermoelectric alloy synthesized via spark plasma sintering. *Physica B: Condensed Matter*, Vol. 622, 2021.

[140] Fan, Z., H. Wang, Y. Wu, X. Liu, and Z. Lu. Thermoelectric performance of PbSnTeSe high-entropy alloys. *Materials Research Letters*, Vol. 5, No. 3, 2017, pp. 187–194.

[141] Liu, Q., G. Wang, Y. Liu, X. Sui, Y. Chen, and S. Luo. Hot deformation behaviors of an ultrafine-grained MoNbTaTiV refractory high-entropy alloy fabricated by powder metallurgy. *Materials Science and Engineering A*, Vol. 809, No. February, 2021, id. 140922.

[142] Wan, Y., Q. Wang, J. Mo, Z. Zhang, X. Wang, X. Liang, et al. WReTaMo refractory high-entropy alloy with high strength at 1600°C. *Advanced Engineering Materials*, Vol. 2100765, 2021, pp. 1–8.

[143] Guo, N. N., L. Wang, L. S. Luo, X. Z. Li, R. R. Chen, Y. Q. Su, et al. Hot deformation characteristics and dynamic recrystallization of the MoNbHfZrTi refractory high-entropy alloy. *Materials Science and Engineering A*, Vol. 651, 2016, pp. 698–707.

[144] Bai, Z. C., X. F. Ding, Q. Hu, M. Yang, Z. T. Fan, and X. W. Liu. The unique deformation behavior and microstructure evolution in high-temperature processing of a low-density TiAlVNb2 refractory high-entropy alloy. *Journal of Alloys and Compounds*, Vol. 885, 2021, pp. 1–12.

[145] Senkov, O. N., J. M. Scott, S. V. Senkova, F. Meisenkothen, D. B. Miracle, and C. F. Woodward. Microstructure and elevated temperature properties of a refractory TaNbHfZrTi alloy. *Journal of Materials Science*, Vol. 47, 2012, pp. 4062–4074.

[146] Jia, Y., L. Zhang, P. Li, X. Ma, L. Xu, S. Wu, et al. Microstructure and mechanical properties of Nb–Ti–V–Zr refractory medium-entropy alloys. *Frontiers in Materials*, Vol. 7, 2020, pp. 1–11.

[147] Eleti, R. R., T. Bhattacharjee, A. Shibata, and N. Tsuji. Unique deformation behavior and microstructure evolution in high temperature processing of HfNbTaTiZr refractory high entropy alloy. *Acta Materialia*, Vol. 171, 2019, pp. 132–145.

[148] Sakai, T., A. Belyakov, R. Kaibyshev, H. Miura, and J. J. Jonas. Dynamic and post-dynamic recrystallization under hot, cold and severe plastic deformation conditions. *Progress in Materials Science*, Vol. 60, No. 1, 2014, pp. 130–207.

[149] Eleti, R. R., A. H. Chokshi, A. Shibata, and N. Tsuji. Unique high-temperature deformation dominated by grain boundary sliding in heterogeneous necklace structure formed by dynamic recrystallization in HfNbTaTiZr BCC refractory high entropy alloy. *Acta Materialia*, Vol. 183, 2020, pp. 64–77.

[150] Abhijit, A., J. Varghese, P. Chalavadi, P. Sai Karthik, K. Bhanu Sankara Rao, and K. V. Rajulapati. Negative strain rate sensitivity in two-phase nanocrystalline CoCrFeMnNi high-entropy alloy with broader grain size distribution studied by nanoindentation. *Transactions of the Indian Institute of Metals*, Vol. 72, No. 10, 2019, pp. 2861–2867.

[151] Rymer, L. M., P. Frint, T. Lindner, G. Gebel, M. Löbel, and T. Lampke. Strain-rate sensitive deformation behavior under tension and compression of Al0.3CrFeCoNiMo0.2. *Advanced Engineering Materials*, Vol. 24, No. 4, 2022, pp. 1–9.

[152] Komarasamy, M., K. Alagarsamy, and R. S. Mishra. Serration behavior and negative strain rate sensitivity of Al0.1CoCrFeNi high entropy alloy. *Intermetallics*, Vol. 84, 2017, pp. 20–24.

[153] Yasuda, H. Y., K. Shigeno, and T. Nagase. Dynamic strain aging of Al0.3CoCrFeNi high entropy alloy single crystals. *Scripta Materialia*, Vol. 108, 2015, pp. 80–83.

[154] Senkov, O. N., S. V. Senkova, and C. Woodward. Effect of aluminum on the microstructure and properties of two refractory high-entropy alloys. *Acta Materialia*, Vol. 68, 2014, pp. 214–228.

[155] Ji, W., Z. Fu, W. Wang, H. Wang, J. Zhang, Y. Wang, et al. Mechanical alloying synthesis and spark plasma sintering consolidation of CoCrFeNiAl high-entropy alloy. *Journal of Alloys and Compounds*, Vol. 589, 2014, pp. 61–66.

[156] Sriharitha, R., B. S. Murty, and R. S. Kottada. Alloying, thermal stability and strengthening in spark plasma sintered AlxCoCrCuFeNi high entropy alloys. *Journal of Alloys and Compounds*, Vol. 583, 2014, pp. 419–426.

[157] Praveen, S., J. Basu, S. Kashyap, and R. S. Kottada. Exceptional resistance to grain growth in nanocrystalline CoCrFeNi high entropy alloy at high homologous temperatures. *Journal of Alloys and Compounds*, Vol. 662, 2016, pp. 361–367.

[158] Pradeep, K. G., N. Wanderka, P. Choi, J. Banhart, B. S. Murty, and D. Raabe. Atomic-scale compositional characterization of a nanocrystalline AlCrCuFeNiZn high-entropy alloy using atom probe tomography. *Acta Materialia*, Vol. 61, No. 12, 2013, pp. 4696–4706.

[159] Sriharitha, R., B. S. Murty, and R. S. Kottada. Phase formation in mechanically alloyed AlxCoCrCuFeNi (x = 0.45, 1, 2.5, 5 mol) high entropy alloys. *Intermetallics*, Vol. 32, 2013, pp. 119–126.

[160] Ang, A. S., C. C. Berndt, M. L. Sesso, A. Anupam, R. S. Kottada, and B. S. Murty. Plasma-sprayed high entropy alloys: Microstructure and properties of AlCoCrFeNi and MnCoCrFeNi. *Metallurgical and Materials Transactions A: Physical Metallurgy and Materials Science*, Vol. 46, No. 2, 2015, pp. 791–800.

[161] Zhang, A., J. Han, J. Meng, B. Su, and P. Li. Rapid preparation of AlCoCrFeNi high entropy alloy by spark plasma sintering from elemental powder mixture. *Materials Letters*, Vol. 181, 2016, pp. 82–85.

[162] Fu, Z., W. Chen, H. Wen, Z. Chen, and E. J. Lavernia. Effects of Co and sintering method on microstructure and mechanical behavior of a high-entropy Al0.6NiFeCrCo alloy prepared by powder metallurgy. *Journal of Alloys and Compounds*, Vol. 646, 2015, pp. 175–182.

[163] Yu, P. F., H. Cheng, L. J. Zhang, H. Zhang, Q. Jing, M. Z. Ma, et al. Effects of high pressure torsion on microstructures and properties of an Al0.1CoCrFeNi high-entropy alloy. *Materials Science and Engineering: A*, Vol. 655, 2016, pp. 283–291.

[164] Wang, B., A. Fu, X. Huang, B. Liu, Y. Liu, Z. Li, et al. Mechanical properties and microstructure of the CoCrFeNiMn high entropy alloy under high strain rate compression. *Journal of Materials Engineering and Performance*, Vol. 25, No. 7, 2016, pp. 2985–2992.

[165] Floriano, R., G. Zepon, K. Edalati, G. L. B. G. Fontana, A. Mohammadi, Z. Ma, et al. Hydrogen storage properties of new A3B2-type TiZrNbCrFe high-entropy alloy. *International Journal of Hydrogen Energy*, Vol. 46, No. 46, 2021, pp. 23757–23766.